Enzymatic Synthesis of Polyesters: a QM/MM study

Pedro R. Figueiredo[a,d], Beatriz C. Almeida[a,d], Daniel F.A.R. Dourado[b], Andreia F. Sousa[c], Armando J. D. Silvestre[c], Alexandra T. P. Carvalho[a]*

ABSTRACT

Modern society is heavily reliant on synthetic polymers, commonly known as plastics; however plastic pollution is causing immeasurable damage to marine and land ecosystems. Better alternatives are actively being sought-after, such as biodegradable polyesters obtained by enzymatic synthesis. However, wild type enzymes still pose fundamental efficiency limitations. Protein reengineering approaches can circumvent those building up highly specific, selective and thermostable variants. Here we compare in detail the catalytic mechanisms for poly(caprolactone) synthesis by the wild type enzymes *Archaeoglobus fulgidus* carboxylesterase (AfEST) and *Candida antarctica* lipase B (CalB) by performing Quantum mechanics calculations and Quantum Mechanics/Molecular Mechanics Molecular Dynamics simulations. We found that bond-forming/breaking events are concerted with a proton transfer to or from the catalytic histidine in all the transition states, but with different degrees of coupling between the motions of the atoms involved. Our results give important insights towards the design of enzyme variants combining good activity with high thermostability in the synthesis of poly(caprolactone), which due to its biodegradability, biocompatibility and permeability characteristics is of great importance for biomedical applications, such as protein delivery, tissue engineering, gene delivery, orthopedic devices and resorbable sutures.

Keywords: Biodegradable polyesters, poly(caprolactone), enzymatic synthesis, carboxylesterase, AfEST, lipase, CalB, QM/MM MD simulations

INTRODUCTION

Synthetic polymers are extensively used by industry and technologies such as in packaging, textiles, electronic devices, machinery, pharmacy and medicine as highly advanced materials.[1] However, in the last years, ecological concerns have stimulated the search for better alternatives to commodity plastics, especially because most of these polymers are non-biodegradable, persisting on the environment. There is, thus, a great urgency to find more sustainable alternatives, since plastic pollution is endangering ecosystems.[2]

Precisely, due to the non-biodegradability of conventional commercial polymers like poly(propylene) and poly(ethylene), the aliphatic-family of polyesters have been in the spotlight due to their ability to biodegrade in a reasonable time-scale.[3] Among aliphatic polyesters, poly(caprolactone) (PCL) deserves a special focus for its biodegradability, biocompatibility, and permeability, meaning that PCL is a good candidate for biomedical applications, such as protein delivery, tissue engineering, gene delivery, orthopedic devices, and resorbable sutures.[4–7] However, widespread commercialization of PCL is hampered due to synthesis and production issues, together with related economic obstacles, although the thermoplastic supply and demand of biodegradables are on high[8] and PCL could be fuelled up.

[a] CNC – Center for Neuroscience and Cell Biology, Institute for Interdisciplinary Research (IIIUC), University of Coimbra, 3004-504 Coimbra, Portugal

[b] Almac Sciences, Department of Biocatalysis and Isotope Chemistry, Almac House, 20 Seagoe Industrial Estate, Craigavon, BT63 5QD, Northern Ireland UK

[c] CICECO – Aveiro Institute of Materials, 3810-193 Aveiro, Portugal

[d] Contributed equally

* atpcarvalho@uc.pt, www.atpcarvalho.pt

Synthesis of polyesters (e.g. PCL), can be performed mainly by two distinct mechanisms: (i) polycondensation polymerization and (ii) ring-opening polymerization (ROP).[3] The polycondensation mechanism has major drawbacks such as high temperatures and long reaction times that favour unwanted side reactions. The reactions are also limited to equilibrium requering water to be removed from the medium.[9] But in the case of reactions performed by ROP, they can be highly efficient because no by-products, such as alcohols, are produced and no substrates need to be activated. This is a significant advantage over polycondensation polymerization both from a green chemistry perspective due to the atom-efficiency, but also because yields and molecular weights are favored.[10,11] Aiming to achieve the desired polymer properties, the ROP mechanism has been continuously refined over the years.[1] Several combinations of initiators and catalysts have been evaluated for ROP synthesis, and enzyme-catalysed ROP was considered one of the most promising approaches.[10,12,13] When compared to conventional chemical routes, enzymatic catalysis gives a more precise construction of well-defined structures, such as high control of enantio-, chemo-, regio-, stereo- and choro-selectivity. More important, enzymes are recyclable, eco-friendly, usually do not require the use of toxic reagents, and avoid the problems associated with trace residues of metallic catalysts.[11,14]

Several lipases (EC 3.1.1.3) and some carboxylesterases (EC 3.1.1.1) have been employed to produce polyesters over different ROP conditions, yielding polymers with a vast array of molecular weights (Mw).[12,15] Among lipases, the immobilized lipase B from *Candida antarctica* (CalB) is one of the most studied.[15–19] Although this enzyme is able to synthesize, in some instances, polyesters with relatively high molecular weights and good yields[20,21] (including PCL), in most cases the polymers have low molecular weights.[22,23] Other factors that limit the industrial application of these enzymes are: (i) the low activity and selectivity for some monomers; (ii) unfavourable compatibility in chemoenzymatic reactions; (iii) low stability under harsh reactions conditions.[24] Regarding the last point, although CalB immobilization increases the stability and reusability of the enzyme, the immobilized enzyme still displays maximum activity at 40 ºC with substantial activity drop at higher temperatures for some substrates.[18] Even when higher catalytic activities are obtained with temperatures in range of 60-80 °C, which happens for many substrates and in low-polarity solvents,[25] higher molecular weight polymers are frequently produced at lower reaction temperatures (40 °C, 45 °C).[18,26,27] Hence, the severe conditions required at the industrial scale can compromise catalysis.

However, rational protein engineering approaches can be employed to address these limitations and expand the scope of enzymes for polyester synthesis by ROP.[26–28] Particularly good starting points for enzyme design are enzymes from thermophiles, which have been recognized as potential catalysts in various biotechnology applications.[29–32] The thermophilic esterase from the hyper-thermophilic archaeon *Archaeoglobus fulgidus* (AfEST) was previously tested for the synthesis of the aliphatic polyester PCL in various organic solvents and solvent-free systems.[33–36] The free form of the enzyme (at a concentration of 25 mg/ml), catalyses the formation of polymer chains with a number-average molecular weight (Mn) of 1400 g/mol and with a monomer conversion of almost 100 %, in toluene at 80 ºC for 72 h.[35] On the other hand, the immobilized form of the enzyme (80 mg), achieves the production of polymer chains with molecular mass (Mn) of 1160 g/mol and monomer conversion of 100 %, in the same conditions.[36] Meaning, that the immobilization process in AfEST does not necessarily produce polymers with higher molecular weights.

Considering PCL as a case-study for aliphatic polyesters synthesis, here, we draw lessons from how CalB and AfEST differently achieve PCL synthesis in the quest to obtain enzymes able to match high conversion with high thermostability. We compare in detail, the catalytic mechanisms of the wild type enzymes by performing Quantum Mechanics/Molecular Mechanics (QM/MM) Molecular Dynamics (MD) simulations and Quantum Mechanics (QM) calculations.

METHODS

Initial Setup and Classical Molecular Dynamics

The initial structures were modelled from CalB (5A71[37], 0.91 Å resolution) and AfEST (1JJI[38], 2.20 Å resolution) crystal structures, and the protonation states assigned with MolProbity.[39] The reactants (**RC**), intermediates (**INT-1**, enzyme activated monomer - **EAM** and **INT-2**) and products (**PC**) were geometry optimized in Gaussian09[40] using B3LYP[41] with the 6-31G(d) basis sets and a Polarizable Continuum Model (PCM)[42] solvent description. Atomic partial charges were calculated resorting to the Restrained Electrostatic Potential (RESP)[43] method from the HF/6-31G(d) single-point energy calculations. The initial position of ε-caprolactone (**ε-Cl**) was obtained by molecular docking. The MD simulations of all intermediates in the reaction profiles were performed using the Amber molecular dynamics program (AMBER18)[44] with the parm99SB[45] and GAFF[46] force fields. All the minima in the catalytic cycle were subjected to 20 ns triplicate simulations with different initial velocities, for a total combined time of 60 ns. Reference structures were calculated for all simulations, based on the structure with the lowest root-mean-square deviation (RMSD) to the average of the simulation.[47] More information can be found in the Supporting information (SI) - Material and Methods.

Quantum Mechanical/Molecular Mechanical (QM/MM) Calculations

The QM/MM calculations[48,49] were performed using the internal semi-empirical hybrid QM/MM functionality implemented in AMBER18[44] with periodic boundary conditions. The initial structures for the calculations were the lowest root-mean-square-deviation structures to the average of the MD simulations of the stationary points. The PM6[50,51] semi-empirical method was employed for the high-level layer and the MM region was described by the Amber parm99SB force field.[45] The reactions were conducted at the optimum temperature for each enzyme (318.15 K for CalB and 353.15 K for AfEST). Corrections were later applied to the obtained PM6 potentials of mean force (PMFs) by performing geometry optimizations of the high-level layer models with the exchange-correlation functional of 6-31G(,d) basis set for B3LYP[41] with Grimme D3 dispersion[52], M06-2X[53] and wB97XD[54], according to Carvalho *et al.* and Bowman *et al.*[55,56] More details and the coordinates for these structures are provided in SI.

Electrostatic embedding[57] was employed and the boundary treated via the link atom approach. Long-range electrostatic interactions were described by an adapted implementation of the Particle Mesh Ewald (PME) method for QM/MM.[58]

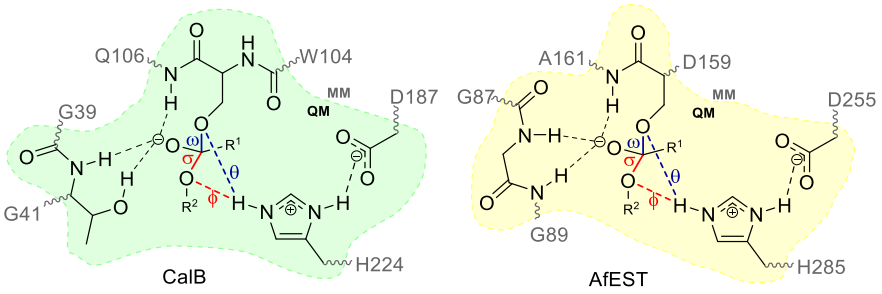

Scheme 1. Representation of the QM region and the corresponding link atoms. **INT-1** $R^1=(CH_2)_5-R^2$. **INT-2** $R^1=(CH_2)_5-OH$, $R^2=(CH_2)_5-CO_2H$.

The high-level layer in the reactants complex (**RC**) for CalB include the ε-caprolactone, S105, the side chains of H224, D187 and T40 and the backbone of Q106 and T40 residues. For AfEST besides the ε-caprolactone and S160, the high-level layer also includes the side chains of H285, D255 and the backbone of G88, G89 and A161 residues (Scheme 1). The total charge of the high-level layer was -1 for both systems. The total number of atoms in the high-level layer in the reactants is 67 for CalB and 63 for AfEST. For the other intermediates, the high-level layer includes the same protein residues plus either the **INT-1**, **EAM**, **INT-2** or the **PCL** model compound.

The potential energy scans of the initial structures (**INT-1** and **INT-2**) were performed along a suitable chosen reaction coordinate restrained in 0.1 Å steps using the umbrella sampling method, except near the transition states were smaller steps of 0.02 Å were employed (Detailed information can be found in the information in SI). The PMFs were computed resorting to the Weighted Histogram Analysis Method (WHAM).[59]

The cluster model transition states where also calculated (with the exchange-correlation functional B3LYP) and vibrational frequency calculations and intrinsic reaction coordinates (IRC) path following were carried out to confirm them.

Unless otherwise stated, all energy values mentioned in the text of this manuscript are given with respect to the PMF corrected with B3LYP/6-31G(d) with Grimme D3 dispersion.

RESULTS AND DISCUSSION

Catalytic Mechanisms of the Wild-type Enzymes

It is well-known that the enzymes CalB and AfEST display the classical α/β hydrolase fold, dimer arrangement and Ser-His-Asp catalytic triad[60,61] (Figure 1). Yet, they are structurally quite distinct. AfEST has a cap domain composed of five helices from two separate regions (residues 1-54 and 188-246),[38] while CalB lacks this structure and has two highly mobile short α-helixes, helix α5 (residues 142-146) and helix α10 (residues 268-287), where the former acts as the putative lid.[37,62] Furthermore, both enzymes display two pockets, an acyl-binding pocket, and a secondary alcohol-binding pocket, with different sizes and orientations[37,38]. The pockets of CalB display a total volume of 204.6 $Å^3$, while the AfEST pockets have an overall volume of 343.5 $Å^3$.[63–65] The CalB catalytic triad is composed of residues S105-H224-D187, which is located close to the putative lid.[37,60,62] AfEST has the catalytic triad S160-H285-D255 and is located at the interface between the classical α/β hydrolase fold and the cap domain.[38] The stated serine act as nucleophiles and the histidine as an acid/base (transferring protons between the catalytic serine and the substrate) that are stabilized by the aspartate residues.[11,66,67] The enzymes also have a region called the oxyanion hole, where a particular spatial arrangement of hydrogen bond donors stabilizes the negative charge that is developed on the oxygen atom of the tetrahedral intermediate structures that are formed during the catalytic mechanism.[67,68] For CalB, the hydrogen bond donors are the backbone amides of T40 and Q106 and the side-chain hydroxyl group of T40,[69] while for AfEST the hydrogen bond donors are the backbone amides of G88, G89 and A161[38] (Figure 1).

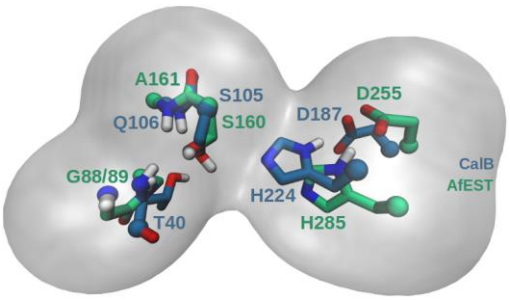

Figure 1. Catalytic triad and oxyanion hole residues of CalB and AfEST.

The first half part of the catalytic cycle or acylation step (Scheme 2), concerns the nucleophilic attack of the serine side-chain oxygen (O_{Ser}) on the carbonyl carbon of the **ε-Cl** substrate, which occurs concomitantly with proton transfer from the O_{Ser} to the histidine residue forming the first tetrahedral intermediate structure (**INT-1**).[70] In the **INT-1** structure, the histidine residue is positively charged and stabilized by the aspartate residue.

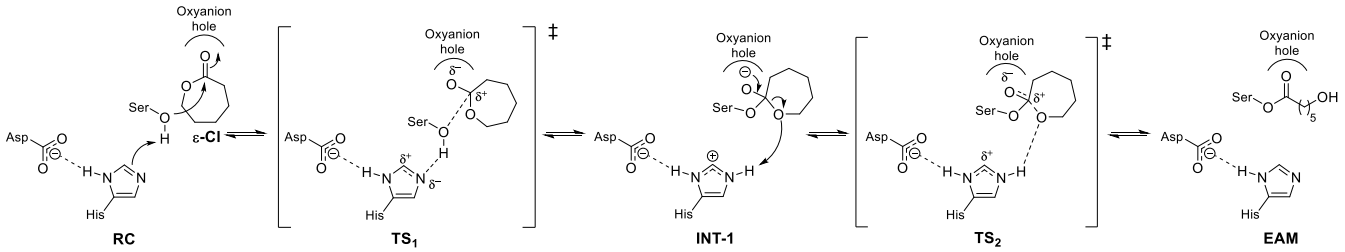

Scheme 2. First half part mechanism for the CalB and AfEST enzymatic synthesis of **PCL**.

For CalB, the **ε-Cl** substrate binds weakly to its active site pocket as is reflected in the high value of K_M of 0.72 M.[71] Accordingly, in the MD simulations we can see that the **ε-Cl** substrate is significantly mobile during the simulations, with the distance between it and the catalytic serine ranging between 3.22 ± 2.30 Å and 9.76 ± 0.81 Å (Figure S1). Consequently, we resorted to model the **INT-1** as our initial structure, which is in accordance with previous studies.[72] Despite the large distance to the serine residue, we can observe in two replicas, that the carbonyl oxygen of the **ε-Cl** substrate establishes a hydrogen bond with the side-chain hydroxyl of the oxyanion-hole residue T40 (Figure 2A). The nucleophilic attack proceeds via the formation of a first transition state structure (**TS_1**), which has a free energy barrier ($\Delta G^{\ddagger}$) of 6.0 ± 0.1 kcal/mol (Figure 3A) generating the **INT-1** (Figure 2B).

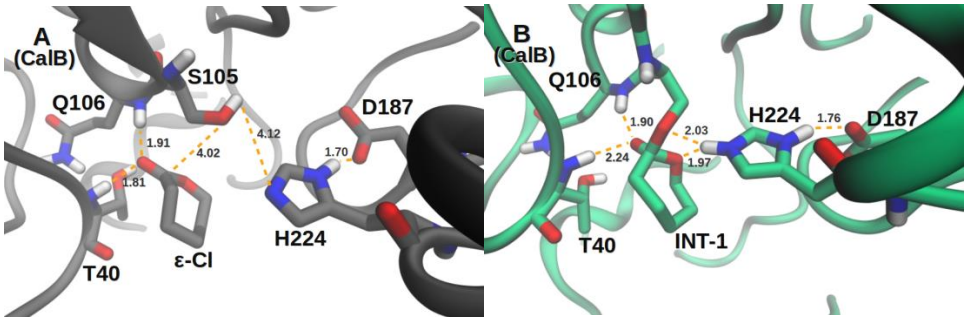

Figure 2. CalB active site pocket: A) **ε-Cl** substrate in the **RC** structure; B) **INT-1** structure.

As previously reported, the **TS_1** and all other transition states in this catalytic cycle are concerted[73,74], meaning that bond making/breaking events occur simultaneously with a proton transfer to or from the histidine. In **INT-1** the backbone amide groups of the oxyanion hole Q106 and T40 stabilize the developing negative charge on the substrate oxygen atom (O_{oxy}) (1.90 ± 0.12 Å and 2.24 ± 0.32 Å, respectively, Figure 2B). This structure has a ΔG of -1.1 ± 0.1 kcal/mol (Figure 3A). The HE atom of H224 is 1.97 ± 0.24 Å from the oxygen atom of the **ε-Cl** substrate (O_{lac}) in the reference structure (Figure 2B). For the AfEST simulations, we observe less variation in the position of **ε-Cl** substrate (Figure 4A and Figure S2), which is also in accordance with the reported K_M of 0.093 M[35] (7.7 fold lower than the one for CalB). The O_{oxy} atom makes a hydrogen bond with the backbone amide group of residue G89 (1.96 ± 0.84 Å, away in the reference structure, Figure 4A). Although the combined size of the pockets is substantially larger in AfEST than in CalB,[70] the **ε-Cl** substrate makes more interactions in AfEST because of its higher hydrophobic nature.[35] The formation of the **INT-1** from the **RC**, proceeds via the **TS_1** with a $\Delta G^{\ddagger}$ of 9.8 ± 0.1 kcal/mol (Figure 3B). We also tested the proton transfer step in a stepwise mechanism. In this case, the serine proton is transferred to the histidine, while the substrate is not correctly positioned for the nucleophilic attack. The barrier associated with this step amounted to 37.0 kcal/mol (with the PM6 semi-empirical method, Figure S3). In **INT-1**, the HE atom is 2.13 ± 0.47 Å from the $O_{lactone}$ atom in the reference structure (Figure 4B) and has a ΔG of 4.4 ± 0.1 kcal/mol (Figure 3B). The amide groups of G88, G89, and A161 make hydrogen bonds with the O_{oxy} atom (distances of 2.28 ± 0.52 Å, 1.70 ± 0.13 Å and 1.95 ± 0.23 Å, respectively), stabilizing the negative charge that has developed in this atom. Furthermore,

the oxygen atoms of D255 interchangeably make hydrogen bonds with the HD atom of the positively charged H285 during the simulations (2.01 ± 0.67 Å, Figure 4B). This interaction highlights the importance of an aspartate residue in the stabilization of the histidine residue.

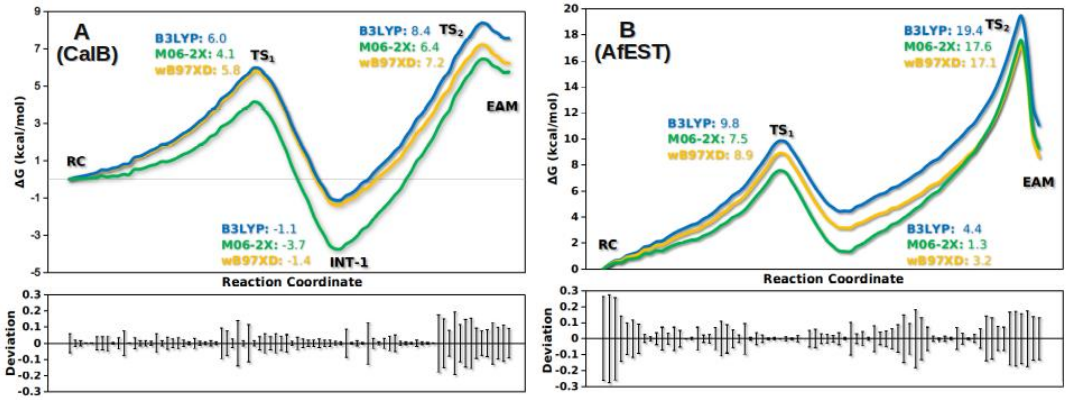

Figure 3. Calculated PMFs for the formation of the **EAM** structure - acylation step - with A) CalB and B) AfEST. Each line denotes the corrected free energies calculated with different theory levels and the statistical uncertainty panel related to the PMF energies. More information can be found in Figures S4 and S5.

The **INT-1** is then converted into the **EAM** by ring-opening and assisted by proton transfer from the histidine residue. In CalB, the second transition state structure (**TS2**) is 8.4 ± 0.1 kcal/mol above the reactants and the overall ΔG‡ for this step is 9.5 kcal/mol (Figure 3A). For AfEST, the **TS2** has an overall $\Delta G^{\ddagger}$ of 19.4 ± 0.2 kcal/mol for the ring-opening (Figure 3B).

For both enzymes the **TS2** show the highest calculated free energy values (including the deacylation steps, that we will detail further in the text). Consequently, the rate-determining step for the enzymatic synthesis of PCL is the formation of the **EAM**, which is in accordance with previous studies.[75,76] According to Eyring's equation,[77] for CalB, the reported turnover number (k_{cat}) of 72.9 s^{-1} for the immobilized form, corresponds to a free energy of about 15.0 kcal/mol at 45 ºC,[71] as for AfEST, the k_{cat} of 0.064 s^{-1} corresponds to a $\Delta G^{\ddagger}$ of 22.7 kcal/mol at 80 ºC.[35] Our calculated barrier of 19.4 ± 0.2 kcal/mol (Figure 3B) for ring-opening is thus in good agreement with experimental data. For CalB only k_{cat} for the imobilized enzyme is available, although we cannot directly compare this value with the free enzyme, the values are in agreement.

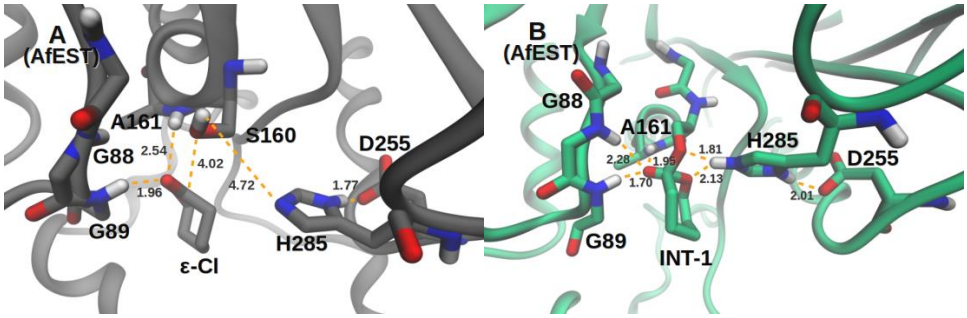

Figure 4. AfEST active site pocket: A) **ε-Cl** substrate in the RC structure; B) **INT-1** structure.

The orientation of the histidine/aspartate residues in the **INT-1** and connected transition states (**TS1** and **TS2**) in the PMFs and in the small cluster models (Figure 2B, Figure **4**B andFigure ***5***) offer an explanation for the enzymes energy differences. As mentioned before, all transition states are concerted, with bond making/breaking events occurring simultaneously with a proton transfer to or from the histidine. In the **INT-1** of AfEST, the HE atom of the H285 residue is closer to the O_{Ser} atom than to the O_{lac} atom (1.85 Å and 3.42 Å, respectively, Figure 5).

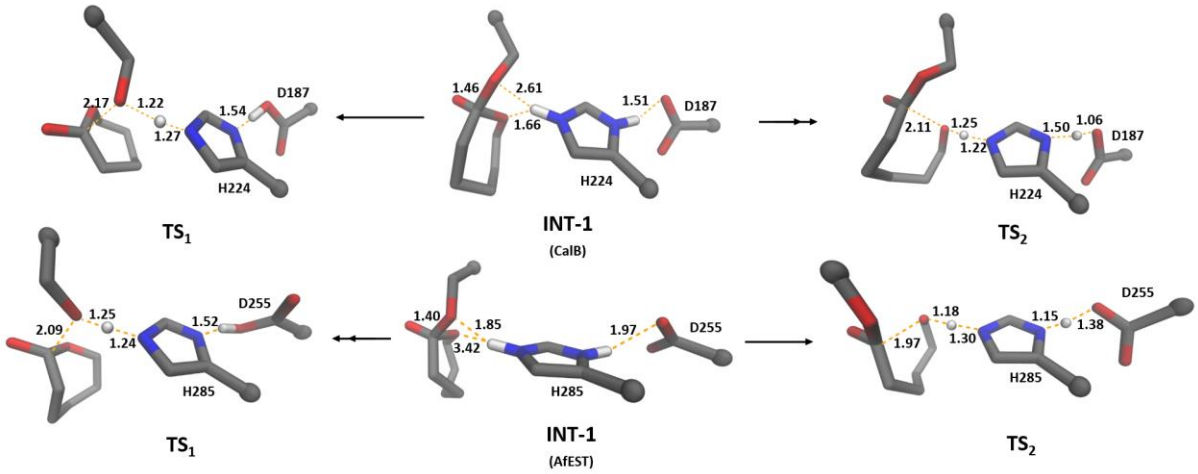

Figure 5. Scheme of the cluster model structures of **TS₁**, **INT-1** and **TS₂** for CalB and AfEST (here, for simplicity, the oxyanion residues were deleted). The same trend observed in the full models is kept in these small models: In **INT-1** the distance from the histidine proton to O_{lac} is smaller for CalB, favouring the forward reaction, whereas in AfEST the distance to O_{Ser} is smaller.

This geometry favours the coupling of vibration motions of the proton transfer to O_{Ser} with bond making to the lactone. In fact, **TS₁** and **INT-1** are close in energy, favouring the reverse reaction (to **TS₁**). In opposition, in CalB the HE atom of H224 is closer to the O_{lac} atom than the O_{Ser} atom (1.66 Å and 2.71 Å, respectively, Figure 5). This leads to a later and higher energy transition state, when going in the reverse direction and much less displacement of the histidine proton in the forward direction (to **EAM**), facilitating concomitant proton transfer and lactone opening, decreasing the overall free energy barrier. Consequently, in CalB the active site arrangement is such that it further promotes O_{lac} leaving, lowering the **TS₂** barrier. On the other hand, in AfEST, the active site arrangement promotes O_{Ser} leaving, making the **INT-1** to **TS₁** backward free energy barrier lower and the overall $\Delta G^{\ddagger}$ is much higher. To further show this, we ran a simulation in which the histidine residue of CalB is in a position similar to the one observed in AfEST. In this simulation, the energy decreases by 4.2 ± 0.1 kcal/mol (Figure S6) as the histidine moves closer to the O_{lac}.

In the second half part of the catalytic cycle (Scheme 3), also called the deacylation step, the second tetrahedral intermediate structure (**INT-2**) is generated after nucleophilic attack by the oxygen atom of the alcohol moiety of a molecule of 6-hydroxycaproic acid (**6-HCA**) to the carbonyl carbon atom of the **EAM**. The **6-HCA** molecule is the initiator (init) for the polymerization reaction and was previously formed in a primary step, with the ring-opening of a molecule of **ε-Cl** and post product hydrolysis.[70] The **PCL** product is formed concomitantly with proton transfer from the histidine to the serine residue, regenerating the free enzyme.

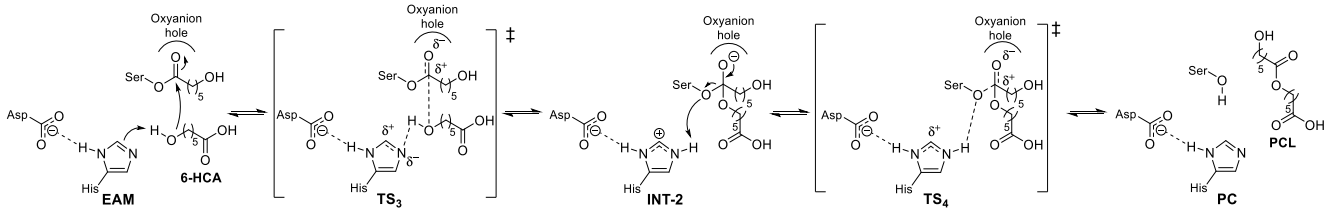

Scheme 3. Second half part mechanism for the CalB and AfEST enzymatic synthesis of **PCL**.

In the reaction catalysed by CalB, the average distance of the carbonyl carbon atom of **EAM** to the hydroxyl oxygen atom of **6-HCA** molecule (O_{init}) is 4.83 ± 0.69 Å and the hydroxyl hydrogen atom of the **6-HCA** molecule is 5.06 ± 1.05 Å away from the NE atom of H224 (Figure 6A and Figure S7). The **INT-2** is generated via the third transition state structure (**TS₃**), which is 7.7 ± 0.2 kcal/mol above the **EAM** (Figure 7A). The hydroxyl hydrogen atom is transferred from the **6-HCA** molecule to the NE atom of H224, while

in a concerted manner a bond is formed between the O_{init} and the carbonyl carbon of the **EAM**, generating the **INT-2** (1.4 ± 0.1 kcal/mol below the **EAM**, Figure 7B and Figure 7A). The reaction proceeds to the **PCL** product release, through the formation of the last transition state structure (**TS_4**, 4.1 kcal/mol above the **INT-2**, Figure 7A), regenerating the free enzyme that is now ready for another turnover (Figure 6C).

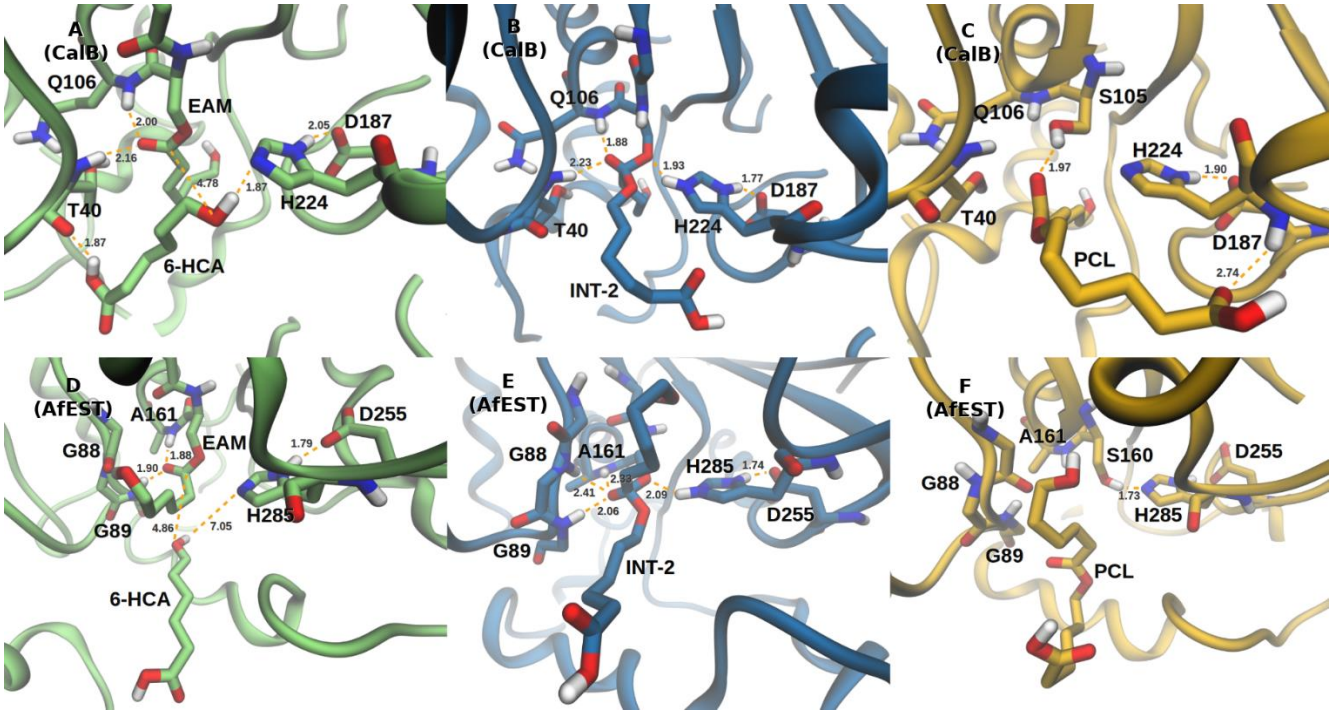

Figure 6. CalB and AfEST active site pockets, respectively: A and D) **EAM** structure with a **6-HCA** molecule; B and E) **INT-2** structure; C and F) Free enzyme with the **PCL** model compound.

In the reaction catalysed by AfEST, the **6-HCA** molecule is in the medium pocket and the O_{init} atom of **6-HCA** molecule 4.86 ± 1.61 Å away from carbonyl carbon atom of the **EAM** (Figure 6D and Figure S8). Bond forming the initiator occurs simultaneously with proton transfer from the HO_{init} atom to H285, as it happens in CalB, with 5.1 ± 0.1 kcal/mol (Figure 7B) being required to reach the **TS_3**. The **INT-2** (Figure 6E) is 10.2 kcal/mol below **TS_3** and 5.1 ± 0.1 kcal/mol below the **EAM** (Figure 7B). The **PCL** product is released after breakage of the CO_{Ser} bond and proton transfer from H285 to the serine oxygen (2.09 ± 0.29 Å away, Figure 6F). This step requires 4.0 kcal/mol (Figure 7B) and after **PCL** product release, the serine hydroxyl side-chain is regenerated.

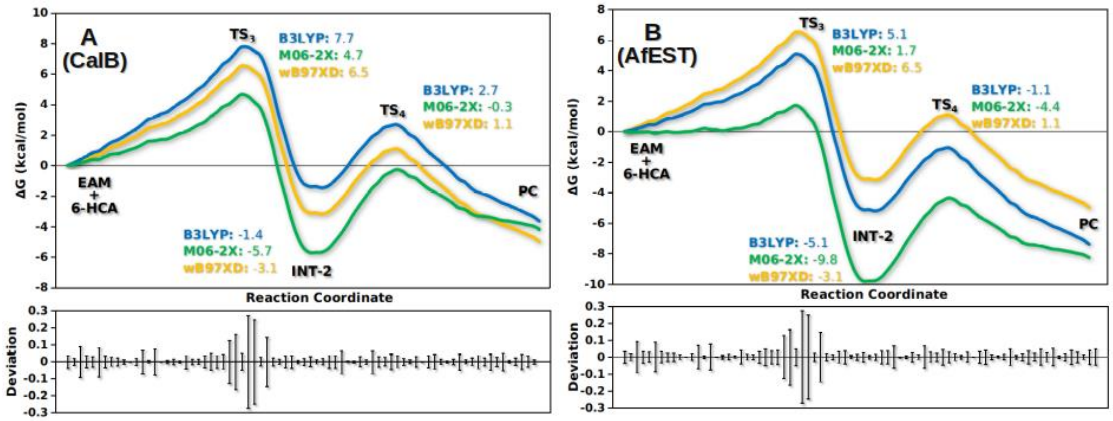

Figure 7. Calculated PMFs for the deacylation - **PCL** product release - with A) CalB and B) AfEST. Each line denotes the corrected free energies calculated with different theory levels and the statistical uncertainty panel related to the PMF energies. More information can be found in Figures S9 and S10.

CONCLUSIONS

We have determined the catalytic mechanisms of the wild type CalB and AfEST enzymes by performing QM/MM and MD simulations. By determining the full catalytic cycles, we showed that the formation of the **EAM** structure is the rate-determining step when ε-caprolactone is the substrate, with the overall barrier for CalB (9.5 kcal/mol) significantly lower than the one for AfEST (19.4 kcal/mol), which is in accordance with the experimental data.[35,71,75,76] Our results also show that the major differences between the enzymes occur exactly during the lactone ring-opening. By comparing the structures, we can observe that the different scaffolds of the enzymes, allow for different arrangements of the catalytic triad residues. Here we showed that these different geometries have important consequences in the way these enzymes convert **ε-Cl**. Since the transition states are concerted (proton transfer occurs concomitantly with CO bond making/breaking), a smaller distance to O_{lac} favours the coupling of the motions of proton transfer to CO_{lac} bond breaking. In opposition, a smaller distance to O_{Ser} favours the coupling of the motions of proton transfer to the CO_{Ser} bond. In accordance, the histidine in AfEST is significantly closer to O_{Ser} favouring transfer in an early transition state in the reverse direction, while in CalB the same proton is closer to the O_{lac}, resulting in the corresponding transition state in the reverse direction and significantly less atom displacement when going in the forward direction leading to a smaller overall free energy barrier.

These insights using PCL as a case-study, and CalB and AfEST to mediate esterification reactions, are useful for protein engineering approaches to tailor the enzymes for industrial important poly(esterification) reactions, especially those affording biodegradable aliphatic polyesters which are gaining momentum due to the search for more sustainable alternatives, since plastic pollution is endangering the environment.

ACKNOWLEDGMENTS

This work was financed by Portuguese national funds via FCT – Fundação para a Ciência e a Tecnologia, under project(s) MIT-Portugal (MIT-EXPL/ISF/0021/2017), the grant IF/01272/2015 and UID/NEU/04539/2019. The costs resulting from the FCT hiring of A.F.S. were funded by national funds (OE), through FCT - Fundação para a Ciência e a Tecnologia, I.P., in the scope of the framework contract foreseen in the numbers 4, 5 and 6 of the article 23 of the Decree-Law 57/2016 of August, changed by Law 57/2017 of 19 July. This work was developed within the scope of the project CICECO - Aveiro Institute of Materials, FCT Ref UID/CTM/50011/2019, financed by national funds through the FCT/MCTES.

REFERENCES

(1) Kobayashi, S.; Makino, A. Enzymatic Polymer Synthesis: An Opportunity for Green Polymer Chemistry. *Chem. Rev.* **2009**, *109*, 5288–5353.

(2) Geyer, R.; Jambeck, J. R.; Law, K. L. Production, Use, and Fate of All Plastics Ever Made. *Science Advances* **2017**, *3*, e1700782.

(3) Vilela, C.; Sousa, A. F.; Fonseca, A. C.; Serra, A. C.; Coelho, J. F. J.; Freire, C. S. R.; Silvestre, A. J. D. The Quest for Sustainable Polyesters – Insights into the Future. *Polym. Chem.* **2014**, *5*, 3119–3141.

(4) Vert, M.; Li, S. M.; Spenlehauer, G.; Guerin, P. Bioresorbability and Biocompatibility of Aliphatic Polyesters. *J Mater Sci: Mater Med* **1992**, *3*, 432–446.

(5) Seyednejad, H.; Ghassemi, A. H.; van Nostrum, C. F.; Vermonden, T.; Hennink, W. E. Functional Aliphatic Polyesters for Biomedical and Pharmaceutical Applications. *Journal of Controlled Release* **2011**, *152*, 168–176.

(6) Siddiqui, N.; Asawa, S.; Birru, B.; Baadhe, R.; Rao, S. PCL-Based Composite Scaffold Matrices for Tissue Engineering Applications. *Molecular Biotechnology* **2018**, *60*, 506–532.

(7) Espinoza, S. M.; Patil, H. I.; San Martin Martinez, E.; Casañas Pimentel, R.; Ige, P. P. Poly-ε-Caprolactone (PCL), a Promising Polymer for Pharmaceutical and Biomedical Applications: Focus on Nanomedicine in Cancer. *International Journal of Polymeric Materials and Polymeric Biomaterials* **2019**, 1–42.

(8) Research, T. M. Polycaprolactone Market to be worth US$ 300 Mn by the end of 2026 - Transparency Market Research http://www.globenewswire.com/news-release/2017/12/04/1220096/0/en/Polycaprolactone-Market-to-be-worth-US-300-Mn-by-the-end-of-2026-Transparency-Market-Research.html (accessed Aug 2, 2019).

(9) Jérôme, C.; Lecomte, P. Recent Advances in the Synthesis of Aliphatic Polyesters by Ring-Opening Polymerization. *Advanced Drug Delivery Reviews* **2008**, *60*, 1056–1076.

(10) Zhang, J.; Shi, H.; Wu, D.; Xing, Z.; Zhang, A.; Yang, Y.; Li, Q. Recent Developments in Lipase-Catalyzed Synthesis of Polymeric Materials. *Process Biochemistry* **2014**, *49*, 797–806.

(11) Douka, A.; Vouyiouka, S.; Papaspyridi, L.-M.; Papaspyrides, C. A Review on Enzymatic Polymerization to Produce Polycondensation Polymers: The Case of Aliphatic Polyesters, Polyamides and Polyesteramides. *Progress in Polymer Science* **2017**, *79*.

(12) Albertsson, A.-C.; Srivastava, R. K. Recent Developments in Enzyme-Catalyzed Ring-Opening Polymerization. *Advanced Drug Delivery Reviews* **2008**, *60*, 1077–1093.

(13) Yang, Y.; Yu, Y.; Zhang, Y.; Liu, C.; Shi, W.; Li, Q. Lipase/Esterase-Catalyzed Ring-Opening Polymerization: A Green Polyester Synthesis Technique. *Process Biochemistry* **2011**, *46*, 1900–1908.

(14) Shoda, S.; Uyama, H.; Kadokawa, J.; Kimura, S.; Kobayashi, S. Enzymes as Green Catalysts for Precision Macromolecular Synthesis. *Chem. Rev.* **2016**, *116*, 2307–2413.

(15) Zhao, H. Enzymatic Ring-Opening Polymerization (ROP) of Polylactones: Roles of Non-Aqueous Solvents. *Journal of Chemical Technology & Biotechnology* **2018**, *93*, 9–19.

(16) Kumar, A.; Gross, R. A. Candida Antartica Lipase B Catalyzed Polycaprolactone Synthesis: Effects of Organic Media and Temperature. *Biomacromolecules* **2000**, *1*, 133–138.

(17) Peeters, J. W.; van Leeuwen, O.; Palmans, A. R. A.; Meijer, E. W. Lipase-Catalyzed Ring-Opening Polymerizations of 4-Substituted ε-Caprolactones: Mechanistic Considerations. *Macromolecules* **2005**, *38*, 5587–5592.

(18) Poojari, Y.; Clarson, S. J. Thermal Stability of Candida Antarctica Lipase B Immobilized on Macroporous Acrylic Resin Particles in Organic Media. *Biocatalysis and Agricultural Biotechnology* **2013**, *2*, 7–11.

(19) Gross, R. A.; Ganesh, M.; Lu, W. Enzyme-Catalysis Breathes New Life into Polyester Condensation Polymerizations. *Trends Biotechnol.* **2010**, *28*, 435–443.

(20) Poojari, Y.; Beemat, J. S.; Clarson, S. J. Enzymatic Synthesis of Poly(ε-Caprolactone): Thermal Properties, Recovery, and Reuse of Lipase B from Candida Antarctica Immobilized on Macroporous Acrylic Resin Particles. *Polymer Bulletin* **2013**, *70*, 1543–1552.

(21) Polloni, A. E.; Veneral, J. G.; Rebelatto, E. A.; de Oliveira, D.; Oliveira, J. V.; Araújo, P. H. H.; Sayer, C. Enzymatic Ring Opening Polymerization of ω-Pentadecalactone Using Supercritical Carbon Dioxide. *The Journal of Supercritical Fluids* **2017**, *119*, 221–228.

(22) Zhao, H.; Nathaniel, G. A.; Merenini, P. C. Enzymatic Ring-Opening Polymerization (ROP) of Lactides and Lactone in Ionic Liquids and Organic Solvents: Digging the Controlling Factors. *RSC Adv.* **2017**, *7*, 48639–48648.

(23) Pellis, A.; Comerford, J. W.; Weinberger, S.; Guebitz, G. M.; Clark, J. H.; Farmer, T. J. Enzymatic Synthesis of Lignin Derivable Pyridine Based Polyesters for the Substitution of Petroleum Derived Plastics. *Nature Communications* **2019**, *10*, 1762.

(24) Yang, J.; Liu, Y.; Liang, X.; Yang, Y.; Li, Q. Enantio-, Regio-, and Chemoselective Lipase-Catalyzed Polymer Synthesis. *Macromolecular Bioscience* **2018**, *18*, 1800131.

(25) Champagne, E.; Strandman, S.; Zhu, X.-X. Recent Developments and Optimization of Lipase-Catalyzed Lactone Formation and Ring-Opening Polymerization https://onlinelibrary.wiley.com/doi/abs/10.1002/marc.201600494 (accessed Jul 31, 2019).

(26) Takwa, M.; Wittrup Larsen, M.; Hult, K.; Martinelle, M. Rational Redesign of Candida Antarctica Lipase B for the Ring Opening Polymerization of d , d -Lactide. *Chemical Communications* **2011**, *47*, 7392–7394.

(27) Montanier, C. Y.; Chabot, N.; Emond, S.; Guieysse, D.; Remaud-Siméon, M.; Peruch, F.; André, I. Engineering of Candida Antarctica Lipase B for Poly(ε-Caprolactone) Synthesis. *European Polymer Journal* **2017**, *95*, 809–819.

(28) Messiha, H. L.; Ahmed, S. T.; Karuppiah, V.; Suardíaz, R.; Ascue Avalos, G. A.; Fey, N.; Yeates, S.; Toogood, H. S.; Mulholland, A. J.; Scrutton, N. S. Biocatalytic Routes to Lactone Monomers for Polymer Production. *Biochemistry* **2018**, *57*, 1997–2008.

(29) Levisson, M.; van der Oost, J.; Kengen, S. W. M. Carboxylic Ester Hydrolases from Hyperthermophiles. *Extremophiles* **2009**, *13*, 567–581.

(30) Elleuche, S.; Schröder, C.; Sahm, K.; Antranikian, G. Extremozymes—Biocatalysts with Unique Properties from Extremophilic Microorganisms. *Current Opinion in Biotechnology* **2014**, *29*, 116–123.

(31) Sarmiento, F.; Peralta, R.; Blamey, J. M. Cold and Hot Extremozymes: Industrial Relevance and Current Trends. *Front. Bioeng. Biotechnol.* **2015**, *3*.

(32) Li, Q.; Li, G.; Yu, S.; Zhang, Z.; Ma, F.; Feng, Y. Ring-Opening Polymerization of ε-Caprolactone Catalyzed by a Novel Thermophilic Lipase from Fervidobacterium Nodosum. *Process Biochemistry* **2011**, *46*, 253–257.

(33) Manco, G.; Giosuè, E.; D'Auria, S.; Herman, P.; Carrea, G.; Rossi, M. Cloning, Overexpression, and Properties of a New Thermophilic and Thermostable Esterase with Sequence Similarity to Hormone-Sensitive Lipase Subfamily from the Archaeon Archaeoglobus Fulgidus. *Archives of Biochemistry and Biophysics* **2000**, *373*, 182–192.

(34) D'Auria, S.; Herman, P.; Lakowicz, J. R.; Bertoli, E.; Tanfani, F.; Rossi, M.; Manco, G. The Thermophilic Esterase from Archaeoglobus Fulgidus: Structure and Conformational Dynamics at High Temperature. *Proteins: Structure, Function, and Bioinformatics* **2000**, *38*, 351–360.

(35) Ma, J.; Li, Q.; Song, B.; Liu, D.; Zheng, B.; Zhang, Z.; Feng, Y. Ring-Opening Polymerization of ε-Caprolactone Catalyzed by a Novel Thermophilic Esterase from the Archaeon Archaeoglobus Fulgidus. *Journal of Molecular Catalysis B: Enzymatic* **2009**, *56*, 151–157.

(36) Ren, H.; Xing, Z.; Yang, J.; Jiang, W.; Zhang, G.; Tang, J.; Li, Q. Construction of an Immobilized Thermophilic Esterase on Epoxy Support for Poly(ε-Caprolactone) Synthesis. *Molecules* **2016**, *21*.

(37) Stauch, B.; Fisher, S. J.; Cianci, M. Open and Closed States of Candida Antarctica Lipase B: Protonation and the Mechanism of Interfacial Activation. *J. Lipid Res.* **2015**, *56*, 2348–2358.

(38) De Simone, G.; Menchise, V.; Manco, G.; Mandrich, L.; Sorrentino, N.; Lang, D.; Rossi, M.; Pedone, C. The Crystal Structure of a Hyper-Thermophilic Carboxylesterase from the Archaeon Archaeoglobus Fulgidus11Edited by R. Huber. *Journal of Molecular Biology* **2001**, *314*, 507–518.

(39) Chen, V. B.; Arendall, W. B.; Headd, J. J.; Keedy, D. A.; Immormino, R. M.; Kapral, G. J.; Murray, L. W.; Richardson, J. S.; Richardson, D. C. MolProbity: All-Atom Structure Validation for Macromolecular Crystallography. *Acta Crystallogr D Biol Crystallogr* **2010**, *66*, 12–21.

(40) Frisch, M.; Trucks, G.; Schlegel, H.; Scuseria, G.; Robb, M.; Cheeseman, J.; Scalmani, G.; Barone, V.; Mennucci, B.; Petersson, G.; Nakatsuji, H.; Caricato, M.; Li, X.; Hratchian, H.; Izmaylov, A.; Bloino, J.; Zheng, G.; Sonnenberg, J.; Hada, M.; Ehara, M.; Toyota, K.; Fukuda, R.; Hasegawa, J.; Ishida, M.; Nakajima, T.; Honda, Y.; Kitao, O.; Nakai, H.; Vreven, T.; Montgomery, J.; Peralta, J.; Ogliaro, F.; Bearpark, M.; Heyd, J.; Brothers, E.; Kudin, K.; Staroverov, V.; Kobayashi, R.; Normand, J.; Raghavachari, K.; Rendell, A.; Burant, J.; Iyengar, S.; Tomasi, J.; Cossi, M.; Rega, N.; Millam, J.; Klene, M.; Knox, J.; Cross, J.; Bakken, V.; Adamo, C.; Jaramillo, J.; Gomperts, R.; Stratmann, R.; Yazyev, O.; Austin, A.; Cammi, R.; Pomelli, C.; Ochterski, J.; Martin, R.; Morokuma, K.; Zakrzewski, V.; Voth, G.; Salvador, P.; Dannenberg, J.; Dapprich, S.; Daniels, A.; Farkas; Foresman, J.; Ortiz, J.; Cioslowski, J.; Fox, D. Gaussian 09, Revision B.01. *Gaussian 09, Revision B.01, Gaussian, Inc., Wallingford CT* **2009**.

(41) Ashvar, C. S.; Devlin, F. J.; Bak, K. L.; Taylor, P. R.; Stephens, P. J. Ab Initio Calculation of Vibrational Absorption and Circular Dichroism Spectra: 6,8-Dioxabicyclo[3.2.1]Octane. *J. Phys. Chem.* **1996**, *100*, 9262–9270.

(42) Tomasi, J.; Mennucci, B.; Cammi, R. Quantum Mechanical Continuum Solvation Models. *Chem. Rev.* **2005**, *105*, 2999–3094.

(43) Bayly, C. I.; Cieplak, P.; Cornell, W.; Kollman, P. A. A Well-Behaved Electrostatic Potential Based Method Using Charge Restraints for Deriving Atomic Charges: The RESP Model. *J. Phys. Chem.* **1993**, *97*, 10269–10280.

(44) Salomon-Ferrer, R.; Case, D. A.; Walker, R. C. An Overview of the Amber Biomolecular Simulation Package: Amber Biomolecular Simulation Package. *Wiley Interdisciplinary Reviews: Computational Molecular Science* **2013**, *3*, 198–210.

(45) Hornak, V.; Abel, R.; Okur, A.; Strockbine, B.; Roitberg, A.; Simmerling, C. Comparison of Multiple AMBER Force Fields and Development of Improved Protein Backbone Parameters. *Proteins* **2006**, *65*, 712–725.

(46) Wang, J.; Wolf, R. M.; Caldwell, J. W.; Kollman, P. A.; Case, D. A. Development and Testing of a General Amber Force Field. *J Comput Chem* **2004**, *25*, 1157–1174.

(47) Dourado, D. F. A. R.; Swart, M.; Carvalho, A. T. P. Why the Flavin Adenine Dinucleotide (FAD) Cofactor Needs To Be Covalently Linked to Complex II of the Electron-Transport Chain for the Conversion of FADH2 into FAD. *Chemistry – A European Journal* **2018**, *24*, 5246–5252.

(48) Warshel, A.; Levitt, M. Theoretical Studies of Enzymic Reactions: Dielectric, Electrostatic and Steric Stabilization of the Carbonium Ion in the Reaction of Lysozyme. *Journal of Molecular Biology* **1976**, *103*, 227–249.

(49) Carvalho, A. T. P.; Barrozo, A.; Doron, D.; Kilshtain, A. V.; Major, D. T.; Kamerlin, S. C. L. Challenges in Computational Studies of Enzyme Structure, Function and Dynamics. *Journal of Molecular Graphics and Modelling* **2014**, *54*, 62–79.

(50) Stewart, J. J. P. Optimization of Parameters for Semiempirical Methods V: Modification of NDDO Approximations and Application to 70 Elements. *J Mol Model* **2007**, *13*, 1173–1213.

(51) Jindal, G.; Warshel, A. Exploring the Dependence of QM/MM Calculations of Enzyme Catalysis on the Size of the QM Region. *J. Phys. Chem. B* **2016**, *120*, 9913–9921.

(52) Grimme, S.; Antony, J.; Ehrlich, S.; Krieg, H. A Consistent and Accurate Ab Initio Parametrization of Density Functional Dispersion Correction (DFT-D) for the 94 Elements H-Pu. *J. Chem. Phys.* **2010**, *132*, 154104.

(53) Zhao, Y.; Truhlar, D. G. The M06 Suite of Density Functionals for Main Group Thermochemistry, Thermochemical Kinetics, Noncovalent Interactions, Excited States, and Transition Elements: Two New Functionals and Systematic Testing of Four M06-Class Functionals and 12 Other Functionals. *Theor Chem Account* **2008**, *120*, 215–241.

(54) Chai, J.-D.; Head-Gordon, M. Long-Range Corrected Hybrid Density Functionals with Damped Atom-Atom Dispersion Corrections. *Phys Chem Chem Phys* **2008**, *10*, 6615–6620.

(55) Carvalho, A. T. P.; Dourado, D. F. A. R.; Skvortsov, T.; de Abreu, M.; Ferguson, L. J.; Quinn, D. J.; Moody, T. S.; Huang, M. Catalytic Mechanism of Phenylacetone Monooxygenases for Non-Native Linear Substrates. *Phys Chem Chem Phys* **2017**, *19*, 26851–26861.

(56) Bowman, A. L.; Grant, I. M.; Mulholland, A. J. QM/MM Simulations Predict a Covalent Intermediate in the Hen Egg White Lysozyme Reaction with Its Natural Substrate. *Chem. Commun. (Camb.)* **2008**, No. 37, 4425–4427.

(57) Bakowies, D.; Thiel, W. Hybrid Models for Combined Quantum Mechanical and Molecular Mechanical Approaches. *J. Phys. Chem.* **1996**, *100*, 10580–10594.

(58) Nam, K.; Gao, J.; York, D. M. An Efficient Linear-Scaling Ewald Method for Long-Range Electrostatic Interactions in Combined QM/MM Calculations. *J. Chem. Theory Comput.* **2005**, *1*, 2–13.

(59) Grossfield, A. *"WHAM: The Weighted Histogram Analysis Method"*, version Revision 7140, June 2005, http://membrane.urmc.rochester.edu/wordpress/?page_id=26.

(60) Uppenberg, J.; Hansen, M. T.; Patkar, S.; Jones, T. A. The Sequence, Crystal Structure Determination and Refinement of Two Crystal Forms of Lipase B from Candida Antarctica. *Structure* **1994**, *2*, 293–308.

(61) Publishers, B. S. *Protein & Peptide Letters*, 6th ed.; Bentham Science Publishers; Vol. 4.

(62) Skjøt, M.; De Maria, L.; Chatterjee, R.; Svendsen, A.; Patkar, S. A.; Østergaard, P. R.; Brask, J. Understanding the Plasticity of the α/β Hydrolase Fold: Lid Swapping on the Candida Antarctica Lipase B Results in Chimeras with Interesting Biocatalytic Properties. *ChemBioChem* **2009**, *10*, 520–527.

(63) Tian, W.; Chen, C.; Lei, X.; Zhao, J.; Liang, J. CASTp 3.0: Computed Atlas of Surface Topography of Proteins. *Nucleic Acids Res* **2018**, *46*, W363–W367.

(64) Figueiredo, P.; Almeida, B. C.; Carvalho, A. T. P. Enzymatic Polymerization of PCL-PEG Co-Polymers for Biomedical Applications. *Front. Mol. Biosci.* **2019**, *6*.

(65) Almeida, B. C.; Figueiredo, P.; Carvalho, A. T. P. Polycaprolactone Enzymatic Hydrolysis: A Mechanistic Study. *ACS Omega* **2019**, *4*, 6769–6774.

(66) Brady, L.; Brzozowski, A. M.; Derewenda, Z. S.; Dodson, E.; Dodson, G.; Tolley, S.; Turkenburg, J. P.; Christiansen, L.; Huge-Jensen, B.; Norskov, L.; Thim, L.; Menge, U. A Serine Protease Triad Forms the Catalytic Centre of a Triacylglycerol Lipase. *Nature* **1990**, *343*, 767.

(67) Bezborodov, A. M.; Zagustina, N. A. Lipases in Catalytic Reactions of Organic Chemistry. *Appl Biochem Microbiol* **2014**, *50*, 313–337.

(68) Simón, L.; Goodman, J. M. Enzyme Catalysis by Hydrogen Bonds: The Balance between Transition State Binding and Substrate Binding in Oxyanion Holes. *J. Org. Chem.* **2010**, *75*, 1831–1840.

(69) Raza, S.; Fransson, L.; Hult, K. Enantioselectivity in Candida Antarctica Lipase B: A Molecular Dynamics Study. *Protein Sci.* **2001**, *10*, 329–338.

(70) Almeida, B. C.; Figueiredo, P.; Carvalho, A. T. P. Polycaprolactone Enzymatic Hydrolysis: A Mechanistic Study. *ACS Omega* **2019**, *4*, 6769–6774.

(71) van der Mee, L.; Helmich, F.; de Bruijn, R.; Vekemans, J. A. J. M.; Palmans, A. R. A.; Meijer, E. W. Investigation of Lipase-Catalyzed Ring-Opening Polymerizations of Lactones with Various Ring Sizes: Kinetic Evaluation. *Macromolecules* **2006**, *39*, 5021–5027.

(72) Escorcia, A. M.; Sen, K.; Daza, M. C.; Doerr, M.; Thiel, W. Quantum Mechanics/Molecular Mechanics Insights into the Enantioselectivity of the O-Acetylation of (R,S)-Propranolol Catalyzed by Candida Antarctica Lipase B. *ACS Catal.* **2017**, *7*, 115–127.

(73) Świderek, K.; Martí, S.; Moliner, V. Theoretical Study of Primary Reaction of Pseudozyma Antarctica Lipase B as the Starting Point To Understand Its Promiscuity. *ACS Catal.* **2014**, *4*, 426–434.

(74) Cen, Y.; Singh, W.; Arkin, M.; Moody, T. S.; Huang, M.; Zhou, J.; Wu, Q.; Reetz, M. T. Artificial Cysteine-Lipases with High Activity and Altered Catalytic Mechanism Created by Laboratory Evolution. *Nat Commun* **2019**, *10*, 1–10.

(75) Kobayashi, S. Enzymatic Ring-Opening Polymerization of Lactones by Lipase Catalyst: Mechanistic Aspects. *Macromolecular Symposia* **2006**, *240*, 178–185.

(76) Poojari, Y.; Beemat, J. S.; Clarson, S. J. Enzymatic Synthesis of Poly(ε-Caprolactone): Thermal Properties, Recovery, and Reuse of Lipase B from Candida Antarctica Immobilized on Macroporous Acrylic Resin Particles. *Polymer Bulletin* **2013**, *70*, 1543–1552.

(77) Evans, M. G.; Polanyi, M. Some Applications of the Transition State Method to the Calculation of Reaction Velocities, Especially in Solution. *Trans. Faraday Soc.* **1935**, *31*, 875–894.

SUPPORTING INFORMATION

Index

Material and Methods S2

Figure S1. Representative structures of **RC** from the MD replicas of CalB. S3

Figure S2. Representative structures of **RC** from the MD replicas of AfEST. S3

Figure S3. Energetic profile for proton transfer (PT) in the stepwise mechanism. S3

Figure S4. Calculated PMF for the acylation step (formation of the **EAM** structure) in CalB. S4

Figure S5. Calculated PMF for the acylation step (formation of the **EAM** structure) in AfEST. S4

Figure S6. Calculated PMF for the ring-opening reaction (**EAM** formation) in CalB when the histidine residue is in a similar position to the one observed in AfEST (**HSP-1**) S5

Figure S7. Representative structures of **EAM** with **6-HCA** from the MD replicas of CalB. S5

Figure S8. Representative structures of **EAM** with **6-HCA** from the MD replicas of AfEST. S5

Figure S9. Calculated PMF for the deacylation step (formation of the **PC** structure) in CalB. S6

Figure S10. Calculated PMF for the deacylation step (formation of the **PC** structure) in AfEST. S6

Figure S11. Superimposition of the **INT-1** structure optimize with PM6 (orange) and B3LYP (green). S6

Figure S12. Histograms for the **INT-1** to **RC** reaction by CalB. S7

Figure S13. Histograms for the **INT-1** to **EAM** reaction by CalB. S7

Figure S14. Histograms for the **INT-2** to **EAM** reaction by CalB. S7

Figure S15. Histograms for the **INT-2** to **PC** reaction by CalB. S7

Figure S16. Histograms for the **INT-1** to **RC** reaction by AfEST. S8

Figure S17. Histograms for the **INT-1** to **EAM** reaction by AfEST. S8

Figure S18. Histograms for the **INT-2** to **EAM** reaction by AfEST. S8

Figure S19. Histograms for the **INT-2** to **PC** reaction by AfEST. S8

Figure S20. IRC paths of: CalB **TS_1** (A, B) and **TS_2** (C, D); AfEST **TS_1** (E, F) and **TS_2** (G, H) S11

Table S1. RC structure coordinates of CalB. S12

Table S2. TS_1 structure coordinates of CalB. S12

Table S3. INT-1 structure coordinates of CalB S13

Table S4. TS_2 structure coordinates of CalB. S13

Table S5. EAM structure coordinates of CalB. S14

Table S6. EAM with **6-HCA** structure of CalB. S14

Table S7. INT-2 structure coordinates of CalB S15

Table S8. PC structure coordinates of CalB S15

Table S9. RC structure coordinates of AfEST. S16

Table S10. TS_1 structure coordinates of AfEST S17

Table S11. INT-1 structure coordinates of AfEST. S17

Table S12. TS_2 structure coordinates of AfEST S17

Table S13. EAM structure coordinates of AfEST S18

Table S14. EAM with a **6-HCA** structure coordinates of AfEST. S18

Table S15. INT-2 structure coordinates of AfEST. S19

Table S16. PC structure coordinates of AfEST. S20

References S21

Material and Methods

Molecular Docking

Molecular docking was performed with AutoDock4.2 suite of programs with the Lamarckian Genetic Algorithm (LGA).[1] A grid box was centred on the oxygen of the catalytic serine side-chain of the (residue 105 for CalB and 160 for AfEST). A total of 100 LGA runs were carried out for each ligand-protein complex. The population was 300, the maximum number of generations was 27,000 and the maximum number of energy evaluations was 2,500,000. These initial structures were used to model the **INT-1** and **INT-2** intermediates.

Molecular Dynamics

The structures were placed within a pre-equilibrated octahedral box of toluene with a distance between the surface of the protein to the box of 10.0 Å. Counter ions were added to make the entire system neutral. The systems were subjected to two initial energy minimizations and to 500 ps of equilibration in an *NVT* ensemble using Langevin dynamics with small restraints on the protein of 10.0 kcal/mol to heat the systems. Production simulations of 50 ns were carried out at 300 K for CalB and 353.15 K for AfEST in the *NPT* ensemble using Langevin dynamics with a collision frequency of 1 ps^{-1}. Constant pressure periodic boundary conditions were imposed with an average pressure of 1 atm. Isotropic position scaling was used to maintain pressure with a relaxation time of 2 ps. The time step was set to 2 fs. SHAKE constraints were applied to all bonds involving hydrogen atoms.[2] The Particle Mesh Ewald (PME) method[3] was used to calculate electrostatic interactions with a cut-off distance of 10.0 Å.

Reaction Coordinates

Two reaction coordinates (Scheme 1) were used in the presented simulations: i) the distance between the tetrahedral carbon and the corresponding oxygen atom (ω and σ); ii) the distance between the histidine proton HE and the corresponding oxygen atom (θ and ϕ). The i) reaction coordinate was used in simulations **INT-1** to **RC** (CalB: 1.4-3.0 Å and AfEST: 1.4-2.8 Å), **INT-1** to **EAM** (CalB: 1.4-3.0 Å) and **INT-2** to **PC** (CalB and AfEST: 1.4-2.5 Å). For the remaining simulations, **INT-1** to **EAM** (CalB: 2.2-1.0 Å and AfEST: 3.4-1.0 Å) and **INT-2** to **EAM** (AfEST: 2.5-1.0 Å), the ii) reaction coordinate was applied. Histograms S12-S15 (CalB) and S16-S19 (AfEST) show that we have adequate sampling in all cases.

PMF corrections

The high-level layer corrections were applied to the calculated PM6 PMFs, following a previously reported protocol.[4] The corrected PMFs free energy can be defined by equation (1) if, at both levels of theory, the interaction energy of the QM/MM does not change significantly:

$$\Delta G_{PMF,corr}(protein) = \Delta G_{PMF,PM6}(protein) + [\Delta G_{B3LYP}(model) - \Delta G_{PM6}(model)] \quad (1)$$

The term $[\Delta G_{B3LYP}(model) - \Delta G_{PM6}(model)]$, is the difference between the free energies for the high-level layer model calculated by B3LYP/6-31G(d) with Grimme D3 dispersion[5] and PM6, respectively.
The free energy for the corrected PMF can be described by equation (2) if the thermal and zero-point energy corrections are considered negligible due to their small quantity:

$$\Delta G_{PMF,corr}(protein) = \Delta G_{PMF,PM6}(protein) + [E_{B3LYP}(model) - E_{PM6}(model)] \quad (2)$$

The term $[E_{B3LYP}(model) - E_{PM6}(model)]$, corresponds to the energetic differences between the stationary points that were optimized through B3LYP/6-31G(d) with the Grimme D3 dispersion correction[5] and PM6, respectively.
The corrections were first performed to the reagents and products of each reaction, and the corrections for the remaining potential surface were interpolated by the addition of an increment factor to each point.

Transition States

The structures of the TSs were obtained from the PM6 PMFs and reoptimized using B3LYP/6-31G(d) with the Grimme D3 dispersion correction[5] and PM6 in the gas phase. All the atoms of the truncated bonds to the protein were kept fixed. The nature of the trasition states was verified by performing frequency calculations and following the intrinsic reaction coordinates (IRCs).

Histidine Simulation

To obtain the structure with the $H224_{CalB}$ in a similar position of $H285_{AfEST}$ (**HSP-1**), we performed a QM/MM simulation with the inverted reaction coordinate in CalB (increasing the distance between the O_{lac} and HE) until the distance between them were similar to the one observed in AfEST (around 3.4 Å). Then, we ran the forward coordinate reaction (reducing the distance between the O_{lac} and HE), also with a QM/MM scan and with the setup already described, using a representative snapshot with the HE_{H224} 3.4 Å away from O_{lac}. The PMFwas computed using WHAM.

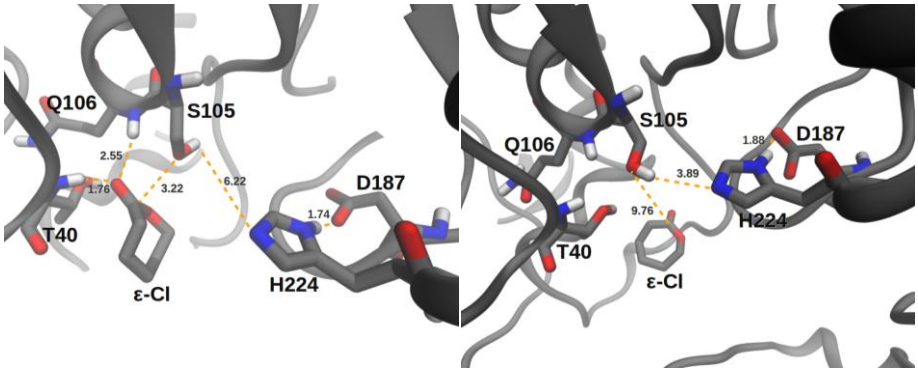

Figure S1. Representative structures of **RC** from the MD replicas of CalB.

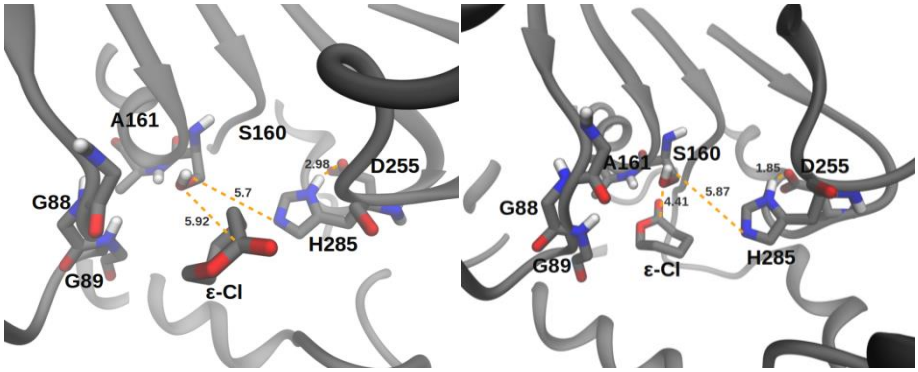

Figure S2. Representative structures of **RC** from the MD replicas of AfEST.

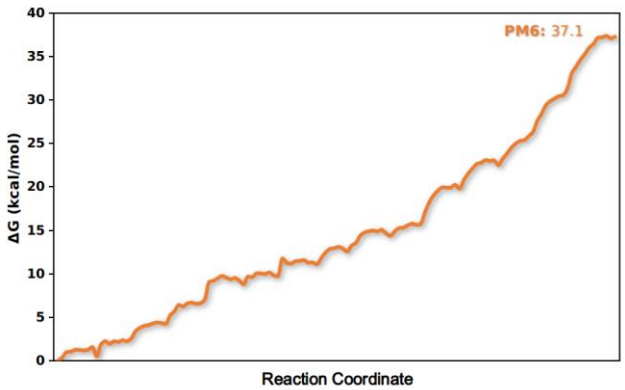

Figure S3. Energetic profile for proton transfer (PT) in the stepwise mechanism. The much higher free energy barrier for the PT of the stepwise mechanism shows that the concerted mechanism is more feasible.

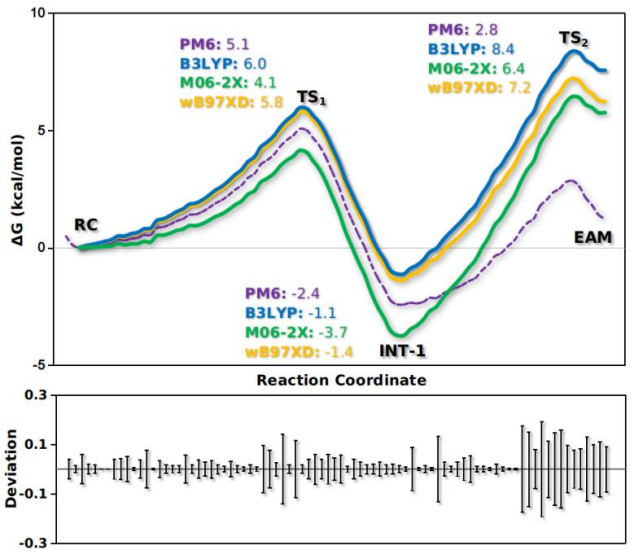

Figure S4. Calculated PMF for the acylation step (formation of the **EAM** structure) in CalB. The dashed line represents the PM6 PMF, the remaining denotes the corrected free energies calculated with different theory levels and the statistical uncertainty panel related to the PMF.

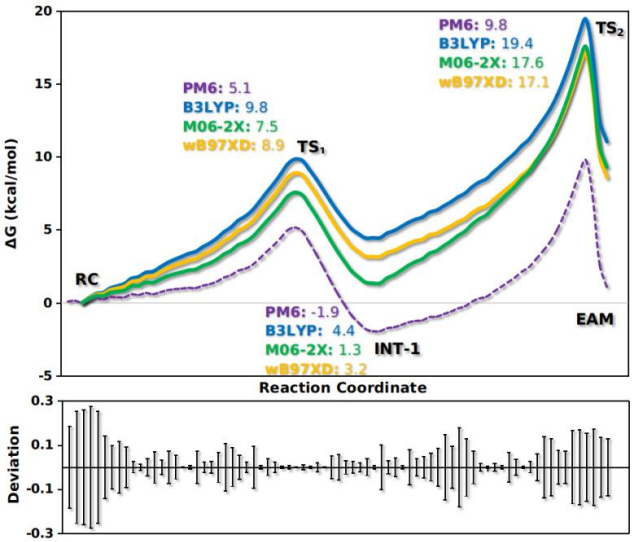

Figure S5. Calculated PMF for the acylation step (formation of the **EAM** structure) in AfEST. The dashed line represents the PM6 PMF, the remaining denotes the corrected free energies calculated with different theory levels and the statistical uncertainty panel related to the PMF.

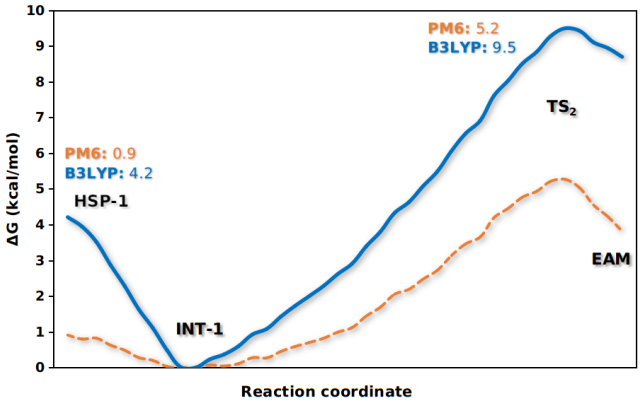

Figure S6. Calculated PMF for the ring-opening reaction (**EAM** formation) in CalB when the histidine residue is in a similar position to the one observed in AfEST (**HSP-1**). The PMF starts with the histidine in the **HSP-1** position (3.4 Å), evolving to the **INT-1** (2.2- 2.1 Å, most stable structure) with the release of 4.2 kcal/mol. Finally, the reaction proceeds to the **EAM** structure through **TS2** with 9.5 kcal/mol. The orange dashed line represents the PM6 PMF and the blue solid line, the corrected PM6 profile with the B3LYP theory level with empirical dispersion.

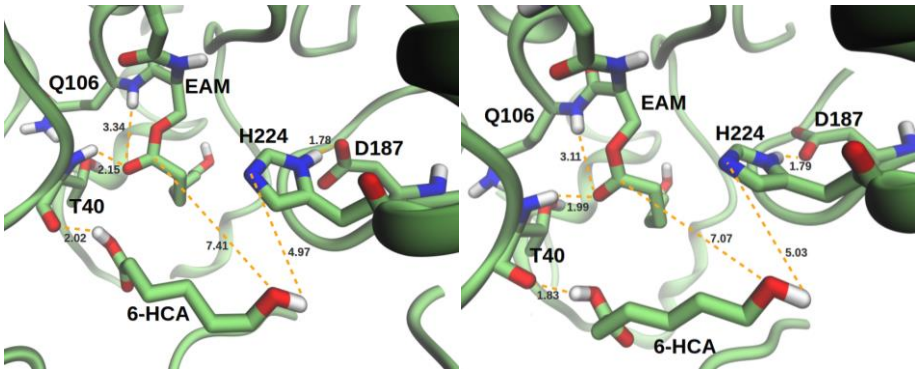

Figure S7. Representative structures of **EAM** with **6-HCA** from the MD replicas of CalB.

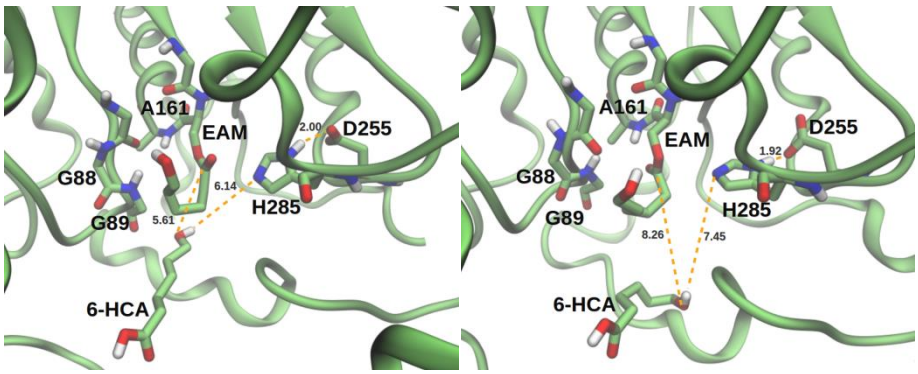

Figure S8. Representative structures of **EAM** with **6-HCA** from the MD replicas of AfEST.

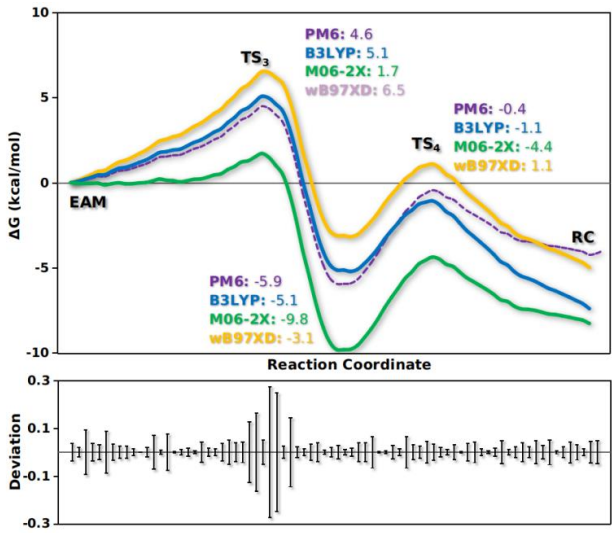

Figure S9. Calculated PMF for the deacylation step (formation of the **PC** structure) in CalB. The dashed line represents the PM6 PMF, the remaining denotes the corrected free energies calculated with different theory levels and the statistical uncertainty panel related to the PMF energies.

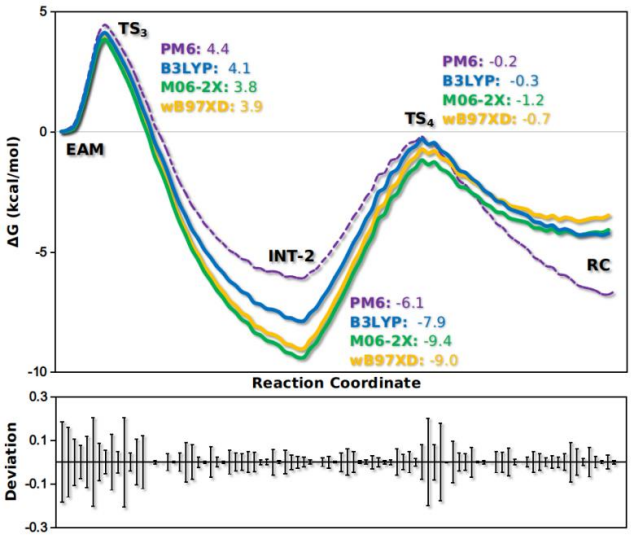

Figure S10. Calculated PMF for the deacylation step (formation of the **PC** structure) in AfEST. The dashed line represents the PM6 PMF, the remaining denotes the corrected free energies calculated with different theory levels and the statistical uncertainty panel related to the PMF.

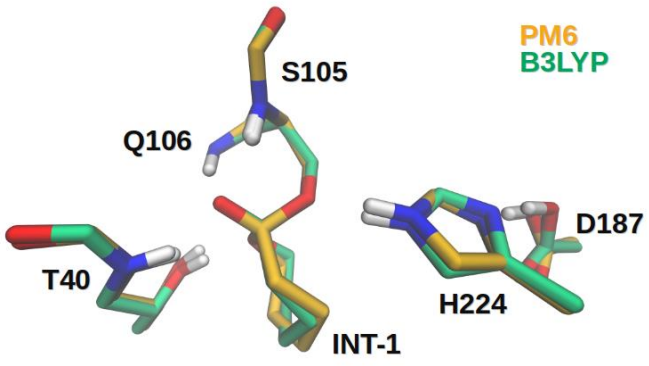

Figure S11. Superimposition of the **INT-1** structure optimize with PM6 (orange) and B3LYP (green).

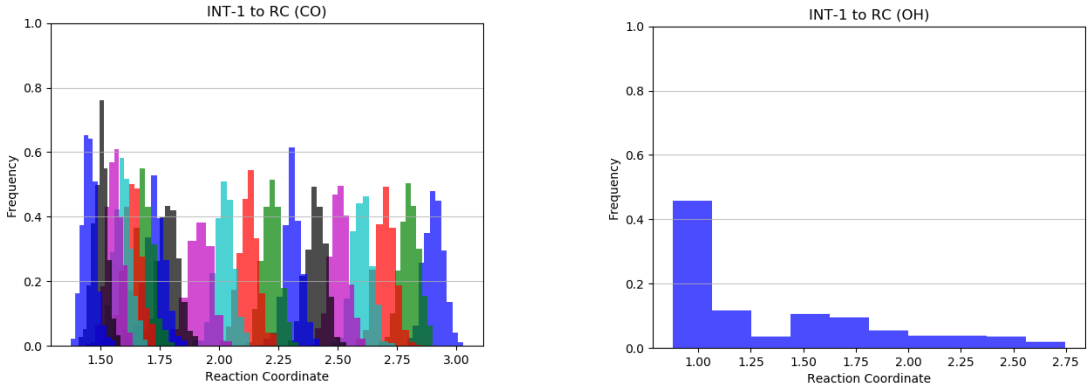

Figure S12. Histograms for the **INT-1** to **RC** reaction by CalB. On the left is the data represented for the i) reaction coordinate and on the right for ii).

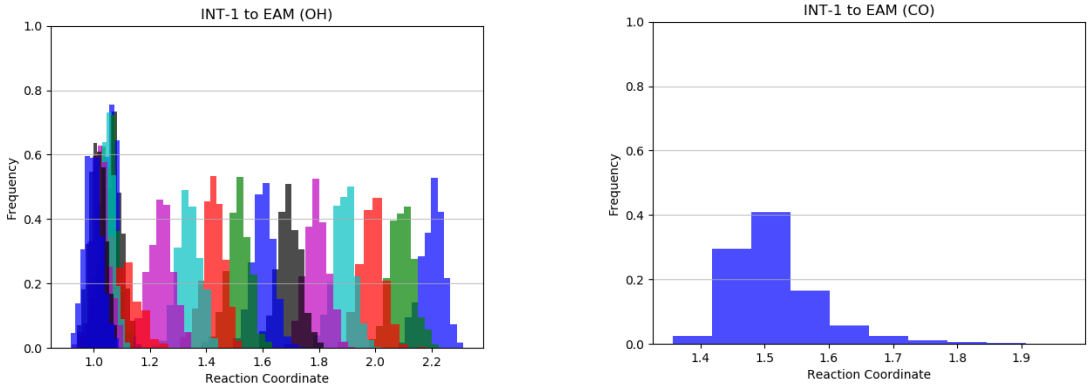

Figure S13. Histograms for the **INT-1** to **EAM** reaction by CalB. On the right is the data represented for the i) reaction coordinate and on the left for ii).

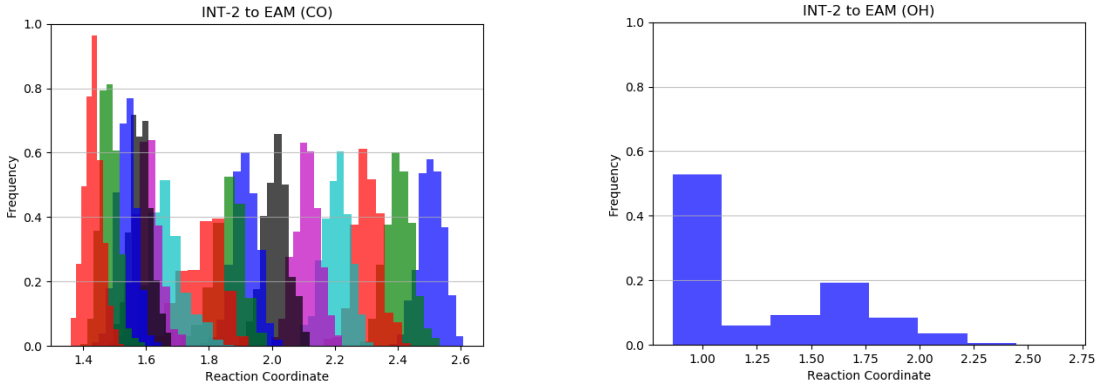

Figure S14. Histograms for the **INT-2** to **EAM** reaction by CalB. On the left is the data represented for the i) reaction coordinate and on the right for ii).

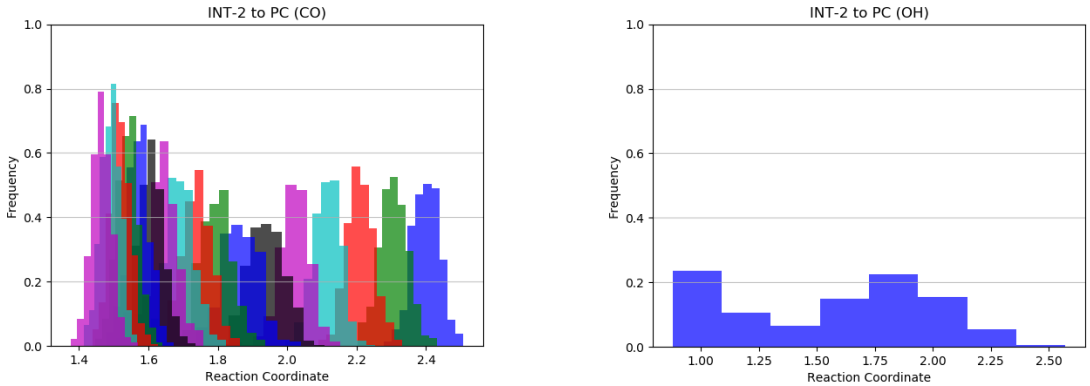

Figure S15. Histograms for the **INT-2** to **PC** reaction by CalB. On the left is the data represented for the i) reaction coordinate and on the right for ii).

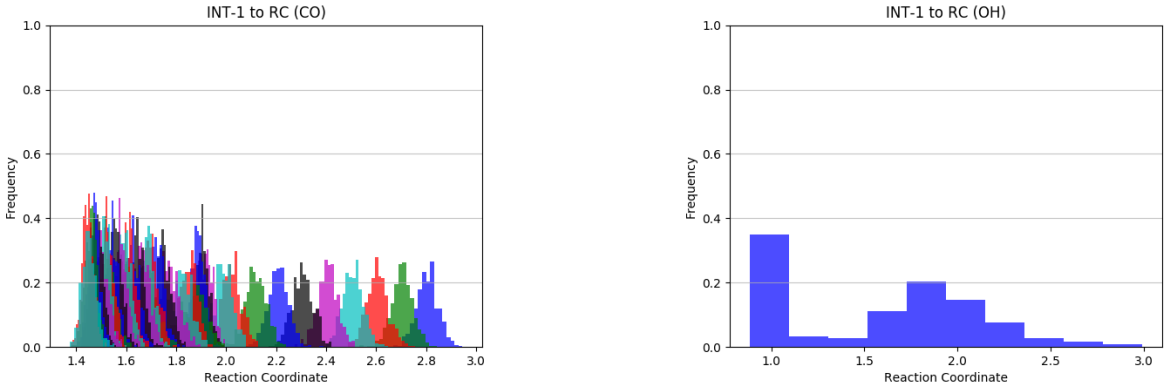

Figure S16. Histograms for the **INT-1** to **RC** reaction by AfEST. On the left is the data represented for the i) reaction coordinate and on the right for ii).

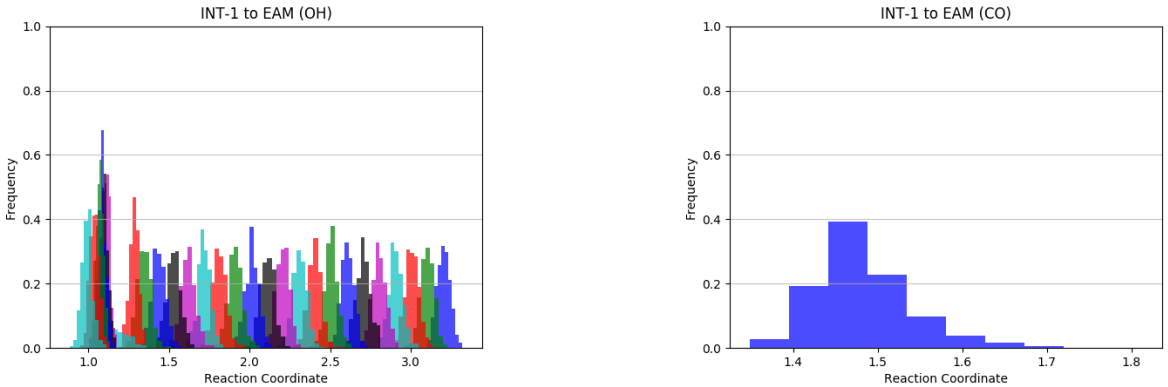

Figure S17. Histograms for the **INT-1** to **EAM** reaction by AfEST. On the right is the data represented for the i) reaction coordinate and on the left for ii).

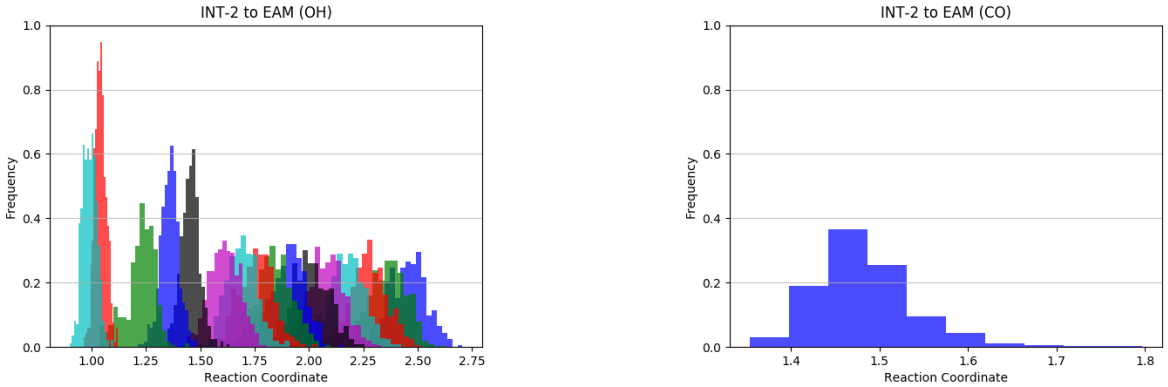

Figure S18. Histograms for the **INT-2** to **EAM** reaction by AfEST. On the right is the data represented for the i) reaction coordinate and on the left for ii).

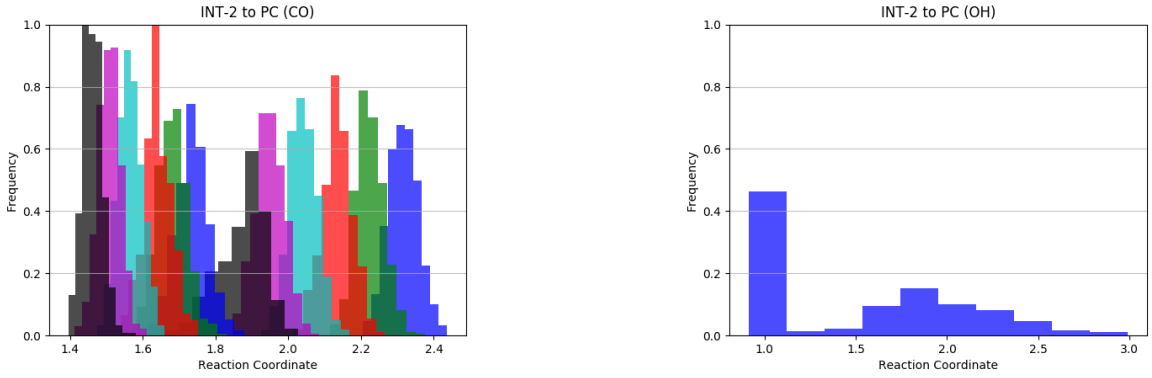

Figure S19. Histograms for the **INT-2** to **PC** reaction by AfEST. On the left is the data represented for the i) reaction coordinate and on the right for ii).

A

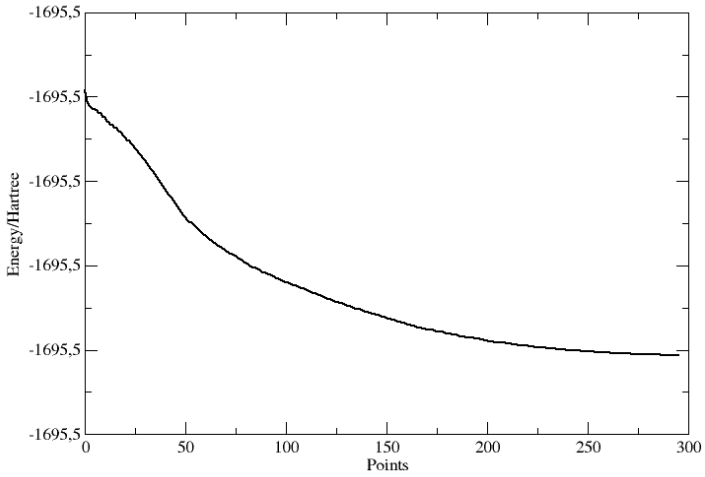
-1695,5
-1695,5
-1695,5
-1695,5
-1695,5
-1695,5
Energy/Hartree
0
50
100
150
200
250
300
Points

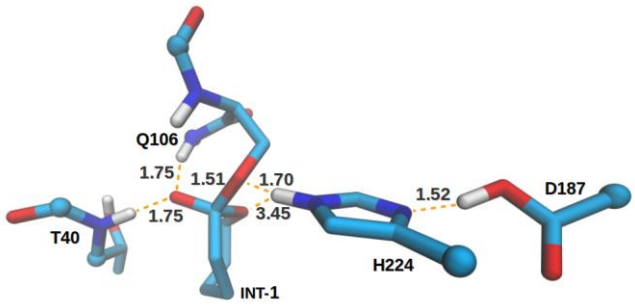
Q106
1.75
1.51
1.70
1.75
3.45
1.52
D187
T40
H224
INT-1

B

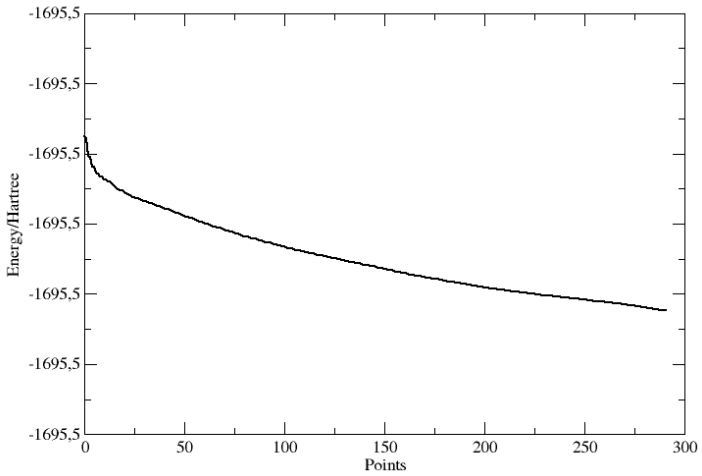
-1695,5
-1695,5
-1695,5
-1695,5
-1695,5
-1695,5
Energy/Hartree
0
50
100
150
200
250
300
Points

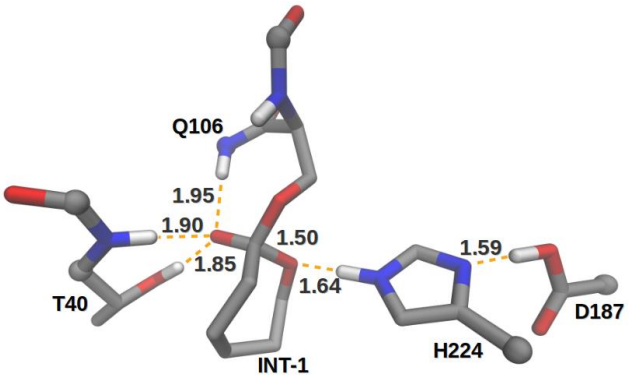
Q106
1.95
1.90
1.50
1.85
1.64
1.59
T40
D187
H224
INT-1

C

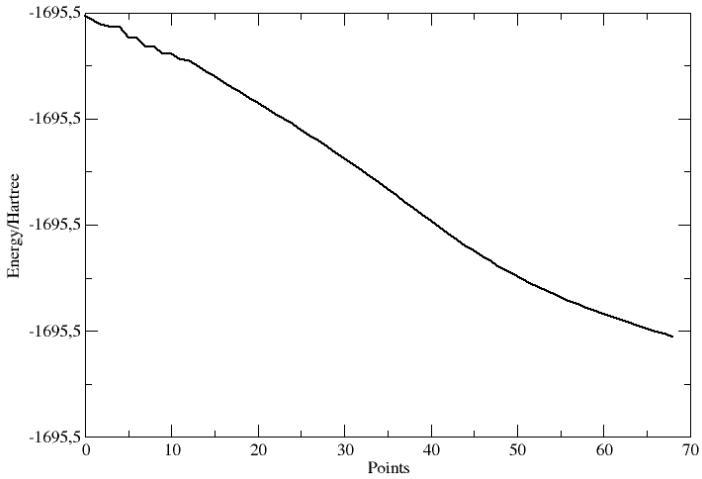
-1695,5
-1695,5
-1695,5
-1695,5
-1695,5
-1695,5
Energy/Hartree
0
10
20
30
40
50
60
70
Points

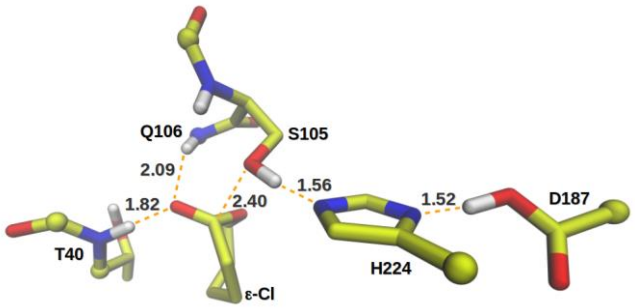
Q106
S105
2.09
1.56
1.82
2.40
1.52
D187
T40
H224
ε-Cl

D

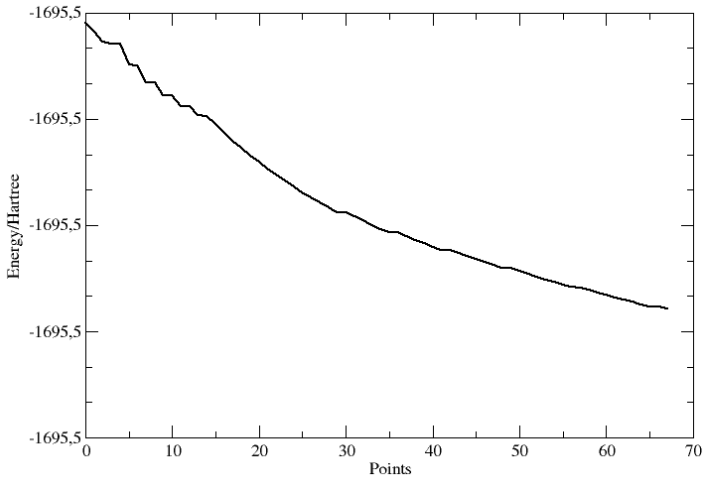
-1695,5
-1695,5
-1695,5
-1695,5
-1695,5
Energy/Hartree
0
10
20
30
40
50
60
70
Points

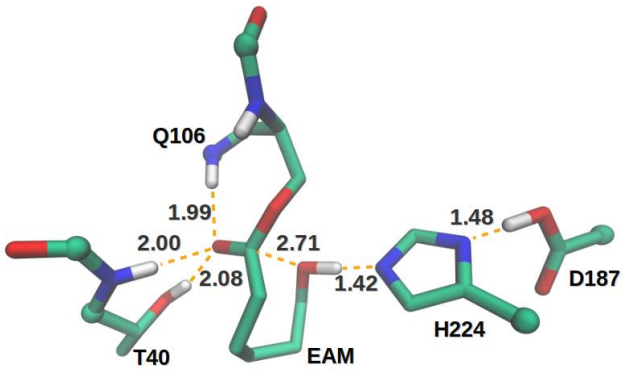
Q106
1.99
2.00
2.71
2.08
1.42
1.48
D187
H224
T40
EAM

E

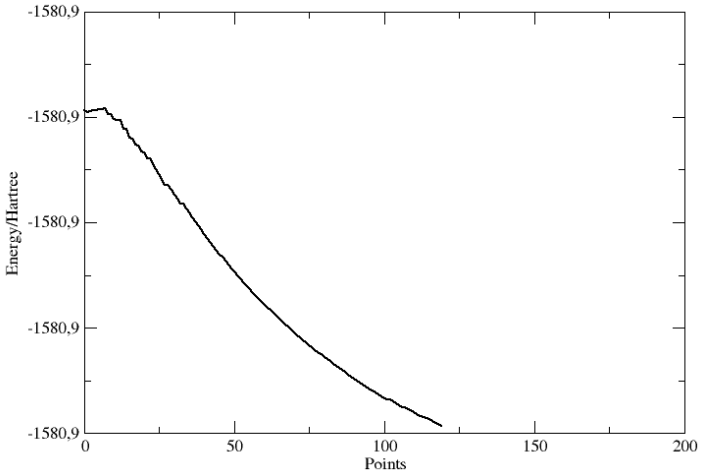
-1580,9
-1580,9
-1580,9
-1580,9
-1580,9
Energy/Hartree
0
50
100
150
200
Points

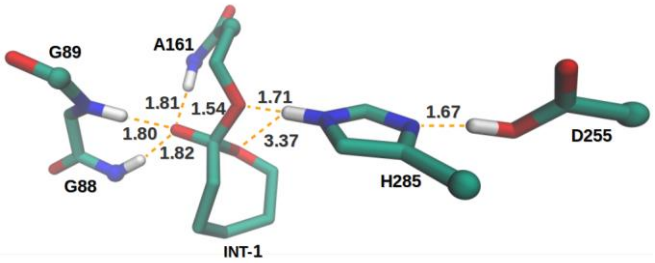
G89
A161
1.81
1.54
1.71
1.80
1.82
3.37
1.67
D255
G88
H285
INT-1

F

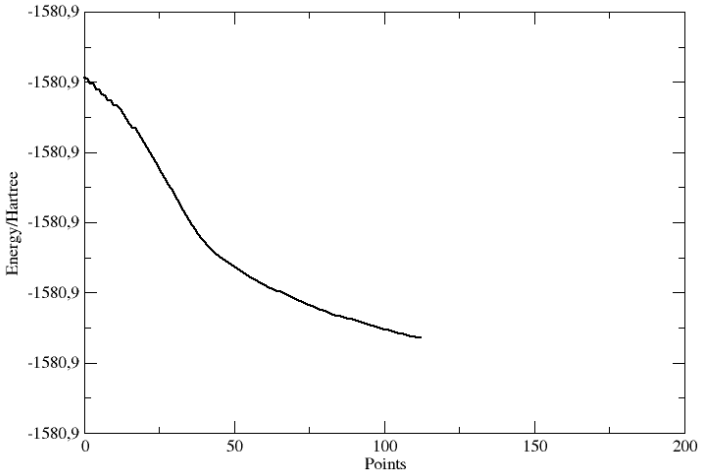
-1580,9
-1580,9
-1580,9
-1580,9
-1580,9
-1580,9
Energy/Hartree
0
50
100
150
200
Points

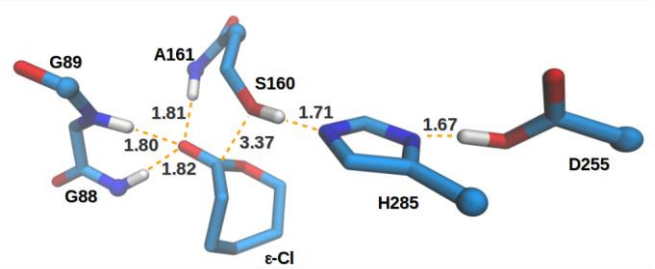
G89
A161
S160
1.81
1.71
1.80
3.37
1.82
1.67
D255
G88
H285
ε-Cl

G

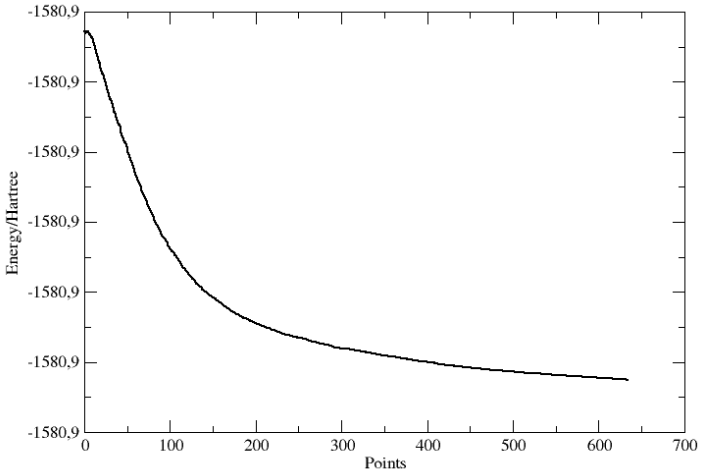

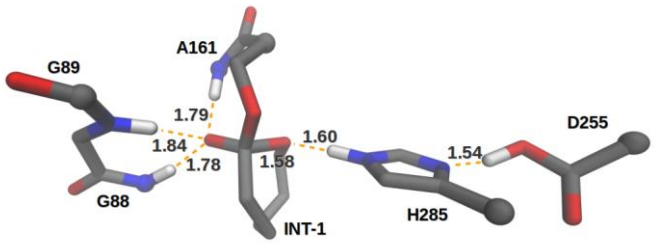

H

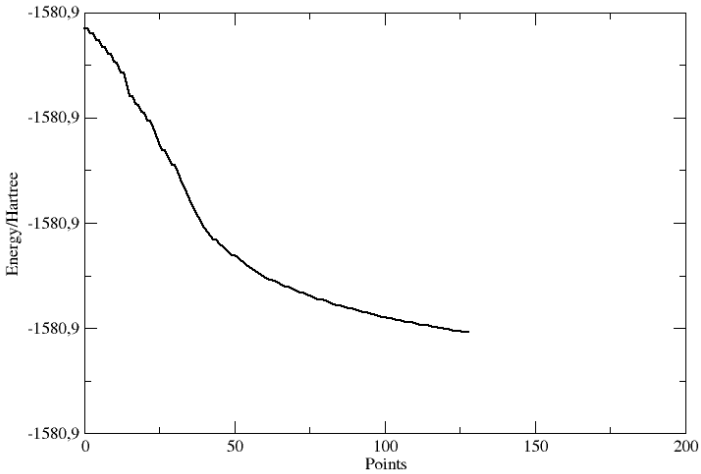

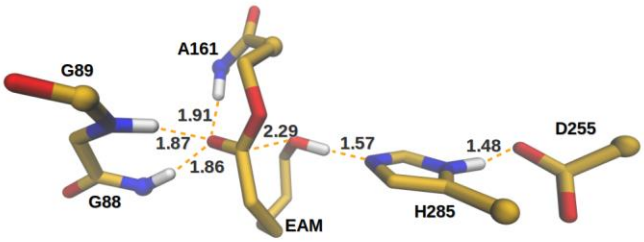

Figure S20. IRC paths of: CalB $\mathbf{TS_1}$ (A, B) and $\mathbf{TS_2}$ (C, D); AfEST $\mathbf{TS_1}$ (E, F) and $\mathbf{TS_2}$ (G, H).

Table S1. RC structure coordinates of CalB.

C	1.497900	-6.984861	-1.609146
O	1.907743	-8.132507	-1.694167
N	2.127357	-5.870285	-2.093918
H	1.565463	-5.024683	-2.067152
C	3.301012	-5.880989	-2.980581
H	3.181578	-6.705704	-3.694782
C	3.487202	-4.550340	-3.760666
H	3.813011	-3.761078	-3.062061
O	2.329066	-4.153031	-4.469728
H	1.707251	-3.766336	-3.826066
C	-3.561731	-3.793040	0.041060
O	-2.453034	-4.270124	-0.171589
N	-4.114751	-2.768583	-0.654878
H	-4.961951	-2.384180	-0.260138
C	-3.370866	-1.850723	-1.537404
H	-4.066661	-1.031828	-1.726326
C	-2.109904	-1.274278	-0.859554
H	-1.323939	-2.023508	-0.929704
H	-1.790507	-0.397071	-1.442279
O	-2.405013	-0.962526	0.486848
H	-1.734183	-0.361975	0.888555
C	-3.128734	-2.448278	-2.964004
O	-3.889579	-2.133840	-3.872523
N	-2.050703	-3.261122	-3.153397
H	-1.530848	-3.653061	-2.378279
C	-0.676630	7.253219	1.808650
H	-1.017495	7.542070	0.808200
H	0.125827	7.923439	2.142821
C	-0.198672	5.788501	1.831165
O	0.415391	5.452729	2.903540
O	-0.464955	5.057276	0.856304
C	0.897279	2.531774	5.286959
H	1.992598	2.423324	5.316510
H	0.493247	1.934386	6.114382
C	0.339982	2.039976	3.971761
N	0.247248	2.854867	2.872094
H	0.404209	3.931891	2.853393
C	-0.238686	2.117723	1.852826
H	-0.442552	2.578888	0.896430
N	-0.460873	0.847645	2.200975
C	-0.096831	0.797864	3.539579
H	-0.179243	-0.119649	4.111296
O	1.216201	-1.558388	-1.367300
O	0.562211	-3.532586	-2.065806
C	2.132946	-1.779194	1.725813
C	1.800604	-3.175700	1.183862
C	2.423217	-0.729812	0.647132
C	0.516700	-3.210715	0.322955
C	1.275893	-0.526571	-0.332451
C	0.754816	-2.778000	-1.108194
H	1.287133	-1.415465	2.323619
H	2.997695	-1.850145	2.398441
H	1.643541	-3.855691	2.029592
H	2.644764	-3.581753	0.608158
H	2.592257	0.237102	1.135907
H	3.331441	-0.981287	0.081094
H	-0.246951	-2.567679	0.780430
H	0.091702	-4.214084	0.271986
H	0.322101	-0.471837	0.196654
H	1.409499	0.389857	-0.909477
H	0.551216	-6.716058	-1.097488
H	4.287237	-4.702819	-4.493351
H	4.212899	-6.083746	-2.400150
H	-4.243473	-4.192769	0.816337
H	-1.937186	-3.669842	-4.070528
H	-1.509559	7.370381	2.516333
H	0.689199	3.600580	5.503210

Table S2. TS$_1$ structure coordinates of CalB.

C	0.484707	2.507913	-4.806968
O	0.543312	2.628209	-6.060135
N	1.557960	2.776208	-3.986143
H	1.444794	2.423704	-3.036274
C	2.931159	3.135683	-4.445506
H	2.827424	3.532327	-5.458344
C	3.503854	4.181564	-3.491970
H	3.582416	3.739667	-2.481856
O	2.731040	5.368051	-3.475570
H	1.804001	5.077028	-3.426532
C	-4.359657	1.785591	-0.817785
O	-5.112159	2.440321	-0.110523
N	-3.068039	1.474396	-0.539370
H	-2.573162	0.790034	-1.107056
C	-2.439283	1.719929	0.746491
H	-3.220172	1.837379	1.502081
C	-1.561502	0.474262	1.095529
H	-0.763213	0.797024	1.781830
H	-2.197542	-0.247010	1.633326
O	-1.045576	-0.140532	-0.057180
C	-1.603631	3.007622	0.854846
O	-1.497168	3.575951	1.936084
O	1.205085	1.204063	0.296687
O	0.374862	1.373280	-1.818098
C	3.581842	0.838994	-1.370228
C	2.981951	-0.546498	-1.028144
C	3.496168	1.856701	-0.210500
C	1.439373	-0.685176	-1.167121
C	2.079972	2.328845	0.133497
C	0.790656	0.655702	-0.905273
H	4.644018	0.705508	-1.612857
H	3.104331	1.242433	-2.273170
H	3.265031	-0.789300	0.002970
H	3.443958	-1.305357	-1.671177
H	3.939394	1.391228	0.680040
H	4.101118	2.744120	-0.447908
H	1.082206	-1.438506	-0.464408
H	1.158678	-0.988028	-2.180679
H	2.059127	2.864362	1.086634
H	1.689329	2.995469	-0.644522
N	-0.983541	3.447851	-0.281272
H	-0.750959	2.767150	-1.002745
C	-1.143856	-6.453391	6.423067
H	-2.194602	-6.652686	6.176599
H	-1.136316	-5.731045	7.247762
C	-0.447543	-5.871511	5.203452
O	0.415779	-6.477767	4.585215
O	-0.920475	-4.673715	4.913472
C	-0.792693	-6.089091	1.581311
H	0.033914	-6.463617	2.193140
H	-0.772106	-6.572224	0.596182
C	-0.712917	-4.594889	1.443803
N	-0.433011	-3.799388	2.533540
H	-0.581830	-4.327865	3.976796
C	-0.471434	-2.546769	2.081531
H	-0.300781	-1.671350	2.695427
N	-0.750013	-2.464289	0.766478
H	-0.919437	-1.320696	0.234201
C	-0.906897	-3.771626	0.352591
H	-1.138712	-4.018228	-0.675515
H	-0.406869	2.179244	-4.250508
H	4.514688	4.461153	-3.811503
H	3.572987	2.243529	-4.471954
H	-4.671022	1.376908	-1.802392
H	-0.284893	4.161234	-0.113735
H	-0.656697	-7.383305	6.728567

H	-1.722016	-6.394116	2.085353

Table S3. INT-1 structure coordinates of CalB.

C	0.776455	3.753976	-5.579862
O	0.870277	4.305194	-6.711599
N	1.869883	3.540841	-4.788158
H	1.635474	3.245075	-3.827968
C	3.263027	4.063883	-5.037106
H	3.197395	5.114991	-5.338698
C	4.077238	3.919876	-3.693004
H	4.264749	2.853613	-3.497048
O	3.463156	4.551010	-2.591840
H	2.644463	4.055402	-2.360721
C	-4.190958	2.987319	-1.633970
O	-4.983833	3.311145	-0.762824
N	-2.888028	2.663280	-1.450260
H	-2.305784	2.426896	-2.244264
C	-2.198507	2.735353	-0.171000
H	-2.914298	2.490459	0.617238
C	-1.033353	1.709107	-0.165206
H	-0.240368	2.053393	0.505572
H	-1.411298	0.749617	0.208667
O	-0.532277	1.477152	-1.475442
C	-1.701743	4.156289	0.151113
O	-2.119220	4.777775	1.122710
O	1.616183	1.285517	-0.654716
O	1.103391	2.996343	-2.152875
C	3.288967	-0.368673	-2.282697
C	2.528154	0.424950	-3.361825
C	3.891467	0.457120	-1.128754
C	1.070170	0.719936	-2.990138
C	3.002032	1.609171	-0.632866
C	0.853171	1.747757	-1.855238
H	2.599942	-1.112995	-1.861785
H	4.103684	-0.939120	-2.748858
H	2.517854	-0.167380	-4.286441
H	3.049637	1.354436	-3.604584
H	4.119163	-0.228310	-0.301141
H	4.848707	0.895377	-1.446271
H	0.588922	-0.221934	-2.698821
H	0.536463	1.103736	-3.867724
H	3.256892	1.860381	0.404433
H	3.164622	2.506335	-1.231794
N	-0.780840	4.635521	-0.722050
H	-0.208917	4.023326	-1.324089
C	-0.772600	-5.092690	5.788190
H	-1.142688	-4.423343	6.573906
H	-0.029057	-5.780586	6.198254
C	-0.165112	-4.285225	4.658440
O	0.969199	-4.464500	4.244773
O	-1.028876	-3.394591	4.186631
C	0.031150	-4.574479	1.102970
H	0.615254	-4.976369	1.938399
H	0.322738	-5.087645	0.178992
C	0.249314	-3.103408	0.980558
N	-0.080620	-2.245152	2.008123
H	-0.622687	-2.888488	3.386359
C	0.252198	-1.032230	1.598497
H	0.128243	-0.117197	2.160094
N	0.778148	-1.060371	0.356660
H	1.116932	-0.222570	-0.151721
C	0.782587	-2.373725	-0.054203
H	1.151963	-2.667320	-1.025241
H	-0.166013	3.394432	-5.132936
H	5.051301	4.403142	-3.839314
H	3.741909	3.492669	-5.842016
H	-4.478012	2.902550	-2.703954
H	-0.359976	5.518593	-0.460779
H	-1.634937	-5.657244	5.412197
H	-1.025533	-4.798989	1.301840

Table S4. TS_2 structure coordinates of CalB.

C	0.066227	2.917050	-4.900265
O	-0.107230	3.329949	-6.035419
N	1.277387	2.814730	-4.237295
H	1.173781	2.533526	-3.264337
C	2.655286	3.291448	-4.617301
H	2.636517	4.382624	-4.730759
C	3.664377	2.894332	-3.543716
H	3.795356	1.804443	-3.540992
O	3.348947	3.385068	-2.252991
H	2.619461	2.858905	-1.871661
C	-4.561657	2.178433	-0.652654
O	-5.214418	2.737362	0.212271
N	-3.286724	1.725539	-0.522015
H	-2.816440	1.325142	-1.323524
C	-2.470668	1.946749	0.663358
H	-3.089317	1.767372	1.546862
C	-1.290081	0.948907	0.678021
H	-0.434896	1.341710	1.228234
H	-1.612127	0.019015	1.152088
O	-0.867822	0.559596	-0.645376
C	-2.002804	3.407866	0.804782
O	-2.359186	4.111359	1.739127
O	1.377756	0.150965	0.618738
O	0.826131	1.928464	-1.341792
C	3.428295	-0.142081	-1.689526
C	2.206645	-0.496534	-2.564458
C	3.506048	-0.731146	-0.271450
C	0.799907	-0.449563	-1.949866
C	2.768346	0.120693	0.774256
C	0.406367	0.776418	-1.145088
H	4.315588	-0.452186	-2.260190
H	3.507647	0.944961	-1.588336
H	2.334660	-1.519172	-2.946299
H	2.226998	0.150936	-3.450311
H	3.127455	-1.762511	-0.245117
H	4.563951	-0.785099	0.026455
H	0.611025	-1.318014	-1.319286
H	0.066834	-0.513489	-2.770271
H	3.014028	-0.268896	1.779305
H	3.170757	1.148082	0.730353
N	-1.184202	3.836034	-0.198043
H	-0.593879	3.176673	-0.707566
C	-1.042820	-6.087691	6.442765
H	-1.372132	-5.359491	7.192547
H	-0.215743	-6.679561	6.840220
C	-0.620623	-5.380597	5.175925
O	0.490939	-5.526950	4.686398
O	-1.594675	-4.629262	4.695718
C	-0.196554	-5.648448	1.488090
H	0.222951	-6.111234	2.387481
H	0.353386	-6.017696	0.614555
C	-0.105150	-4.160982	1.580993
N	-0.755553	-3.461678	2.570907
H	-1.275155	-4.134108	3.814558
C	-0.403656	-2.187682	2.402879
H	-0.729265	-1.379433	3.045160
N	0.421549	-2.007699	1.358681
H	0.896062	-0.942561	0.994394
C	0.616001	-3.262619	0.826926
H	1.252754	-3.426460	-0.032138
H	-0.756157	2.546608	-4.256648
H	4.631118	3.335609	-3.813686
H	2.931534	2.855368	-5.584211
H	-4.968613	1.956076	-1.661597

H	-0.766894	4.744989	-0.037109
H	-1.897931	-6.742229	6.237629
H	-1.237635	-5.985333	1.393988

Table S5. EAM structure coordinates of CalB.

C	-1.412475	6.590371	0.175435
O	-1.446093	7.805944	0.125544
N	-0.943780	5.942428	1.309718
H	-0.970798	4.929839	1.261898
C	-0.830910	6.544388	2.694774
H	-1.608771	7.308516	2.784040
C	-1.023216	5.391135	3.694973
H	-0.096690	4.803709	3.736614
O	-2.140483	4.563597	3.438692
H	-1.886991	3.917810	2.754973
C	-3.262190	2.241549	-3.694979
O	-3.142426	3.292097	-3.084536
N	-3.007551	1.007880	-3.175862
H	-3.347565	0.209291	-3.693869
C	-2.825409	0.831299	-1.735594
H	-2.740212	-0.245518	-1.561249
C	-1.509905	1.476509	-1.296081
H	-0.701481	1.157536	-1.957789
H	-1.573503	2.564052	-1.278200
O	-1.149648	0.953357	0.001546
C	-4.126824	1.274688	-1.018508
O	-5.186372	0.753490	-1.342629
O	1.961180	6.065249	0.479950
O	-1.304533	2.932636	1.061479
C	1.980810	2.504823	1.880070
C	0.816161	2.060225	2.808075
C	2.226992	4.034166	1.844695
C	-0.146069	1.075355	2.128478
C	1.913243	4.643390	0.472130
C	-0.915819	1.760937	1.025353
H	2.892658	1.984328	2.193240
H	1.788385	2.131721	0.864376
H	0.232703	2.924707	3.140155
H	1.208229	1.586415	3.715649
H	1.602990	4.544862	2.590199
H	3.264752	4.281431	2.100559
H	-0.878768	0.686988	2.851334
H	0.395776	0.236735	1.682054
H	2.651852	4.295606	-0.260390
H	0.929624	4.283405	0.131875
H	1.083240	6.349753	0.785755
N	-4.017971	2.218209	-0.054800
H	-3.162416	2.722172	0.146696
C	0.759882	-6.538873	-2.859398
H	0.434375	-6.441158	-3.904377
H	-0.143685	-6.710671	-2.258804
C	1.451002	-5.230189	-2.405995
O	2.643784	-5.292372	-2.043311
O	0.701143	-4.198912	-2.459514
C	4.221184	-2.434006	-1.778028
H	3.904397	-3.485548	-1.790919
H	5.085075	-2.311261	-1.111656
C	3.077504	-1.573304	-1.326872
N	1.772343	-1.975994	-1.483774
H	1.420858	-2.910011	-1.890446
C	0.989411	-0.993014	-0.984802
H	-0.088554	-1.076339	-0.956980
N	1.688046	0.036550	-0.513445
C	3.002009	-0.329630	-0.728016
H	3.820623	0.318815	-0.435878
H	-1.674601	5.901510	-0.647963
H	-1.170112	5.825416	4.691842
H	0.151974	7.011187	2.831989
H	-3.565316	2.194941	-4.759026
H	-4.877495	2.542647	0.367029
H	1.435193	-7.396483	-2.765408
H	4.549474	-2.169776	-2.795188

Table S6. EAM with **6-HCA** structure of CalB.

C	0.716311	-3.521729	-5.816590
O	0.489421	-3.825483	-6.961616
N	-0.091357	-3.787428	-4.732603
H	0.294005	-3.475149	-3.849291
C	-1.415696	-4.455015	-4.689313
H	-1.353622	-5.432061	-5.186489
C	-1.837076	-4.625904	-3.234358
H	-2.792669	-5.157117	-3.191104
O	-2.051404	-3.370764	-2.580362
H	-1.203129	-2.893294	-2.559533
C	6.155660	-2.400231	-3.376340
O	5.308422	-2.821756	-4.152834
N	6.003505	-2.367449	-2.023040
H	6.762868	-1.980967	-1.479201
C	4.769749	-2.686773	-1.291976
H	4.984572	-2.449477	-0.248179
C	3.592821	-1.799150	-1.729298
H	3.824326	-0.737330	-1.597351
H	3.280169	-1.987935	-2.755983
O	2.528907	-2.119121	-0.802138
C	4.428108	-4.213923	-1.223039
O	4.811866	-4.868174	-0.265562
O	-0.060740	-2.877890	4.140860
O	1.048486	-2.572040	-2.447852
C	0.204675	-5.302025	1.203883
C	0.898538	-4.647889	0.002209
C	0.570796	-4.620345	2.538682
C	0.522360	-3.157423	-0.167352
C	-0.489745	-3.621743	3.013543
C	1.360522	-2.573276	-1.267802
H	-0.886013	-5.283676	1.058375
H	0.497579	-6.358801	1.228700
H	0.645530	-5.179416	-0.924282
H	1.984375	-4.727463	0.135538
H	0.720620	-5.359357	3.334202
H	1.529120	-4.090193	2.426035
H	0.720574	-2.611697	0.757784
H	-0.536299	-3.067160	-0.430878
H	-0.796316	-2.959043	2.188916
H	-1.387267	-4.165475	3.331936
H	0.658572	-2.295369	3.851845
N	3.612160	-4.739140	-2.196840
H	3.628132	-4.285323	-3.106032
C	3.995739	4.745388	5.922698
H	4.681222	4.079692	6.461777
H	3.271238	5.189895	6.614701
C	3.271365	3.993577	4.777245
O	3.981677	3.111382	4.185484
O	2.104990	4.341444	4.502414
C	2.975420	5.163804	1.552098
H	2.354772	5.110013	2.454611
H	2.552818	5.882793	0.839292
C	3.081844	3.810188	0.921026
N	3.253616	2.679973	1.681382
H	3.430553	2.729571	2.744094
C	3.303593	1.629400	0.827323
H	3.423451	0.608890	1.171392
N	3.179833	1.991058	-0.446250
C	3.043909	3.368773	-0.385977
H	2.930614	3.966656	-1.284245
H	1.520440	2.335817	-1.951705
O	0.762501	1.920901	-2.402044

C	0.303918	0.898855	-1.532406
H	-0.190840	1.327205	-0.642170
H	1.147114	0.293157	-1.169248
C	-0.691349	0.022420	-2.289065
H	-0.173487	-0.435918	-3.139674
C	-1.923000	0.793460	-2.770026
H	-1.595375	1.596960	-3.440416
C	-2.956505	-0.090817	-3.482120
H	-2.400856	1.276236	-1.905811
C	-2.407714	-0.715601	-4.780597
H	-3.848784	0.506642	-3.713985
H	-3.266369	-0.891298	-2.791893
C	-3.467063	-1.314506	-5.694200
H	-1.874203	0.035013	-5.371205
H	-1.689861	-1.508623	-4.534498
O	-3.499944	-1.170596	-6.891049
O	-4.425919	-2.081257	-5.089489
H	-4.308060	-2.067990	-4.125880
H	-1.012960	-0.795546	-1.624734
H	1.632630	-2.986178	-5.491554
H	-1.082940	-5.220756	-2.693960
H	-2.164409	-3.853030	-5.218965
H	7.140229	-2.018236	-3.702707
H	3.543584	-5.749482	-2.195562
H	4.597708	5.556612	5.487615
H	3.962288	5.534722	1.865876

Table S7. INT-2 structure coordinates of CalB.

C	-6.194660	-1.843297	-2.576691
O	-7.245062	-1.764598	-3.206214
N	-5.944428	-1.221964	-1.383146
H	-4.939493	-1.282350	-1.163971
C	-6.832058	-0.231007	-0.789082
H	-7.784174	-0.683444	-0.545057
C	-6.330148	0.303782	0.552337
H	-5.430531	0.927702	0.406469
O	-6.075312	-0.732259	1.491036
H	-5.552729	-1.404924	1.024430
C	-1.361521	-5.384824	-3.038433
O	-0.710982	-6.367901	-2.714287
N	-1.503205	-4.241811	-2.314305
H	-2.162424	-3.525231	-2.612799
C	-1.028440	-4.119623	-0.946068
H	-0.167806	-4.780916	-0.829318
C	-0.590391	-2.653705	-0.646769
H	-0.735013	-2.441872	0.422093
H	0.480905	-2.569546	-0.861583
O	-1.178279	-1.667328	-1.465589
C	-2.052559	-4.579723	0.104337
O	-1.723403	-5.302023	1.042515
O	0.092219	0.193300	4.921188
O	-2.320861	-0.039402	-2.298863
C	-1.722537	1.247422	1.746630
C	-1.749682	0.748465	0.298267
C	-0.870340	0.368608	2.665457
C	-2.640035	-0.479230	0.084912
C	-0.815405	0.909270	4.090635
C	-2.501855	-1.105399	-1.322859
H	-1.315265	2.268652	1.771984
H	-2.749570	1.307402	2.138323
H	-0.728183	0.517040	-0.030378
H	-2.102564	1.550103	-0.359074
H	-1.265729	-0.658693	2.680650
H	0.154781	0.313071	2.274681
H	-3.686756	-0.198721	0.242646
H	-2.430268	-1.262275	0.823984
H	-0.452045	1.943903	4.080662
H	-1.830842	0.921348	4.524541
H	-0.174211	-0.738749	4.886616
O	-3.439494	-1.953591	-1.662143
C	-3.489602	0.684336	-2.624116
H	-4.256766	0.014596	-3.028624
H	-3.910007	1.170379	-1.724266
C	-3.084425	1.738143	-3.648191
H	-3.975244	2.292907	-3.974870
C	-2.016412	2.696797	-3.109259
H	-1.240578	2.108671	-2.609121
C	-1.369117	3.533178	-4.211549
H	-2.456274	3.356464	-2.346294
C	-0.167426	4.336788	-3.685320
H	-2.106456	4.212136	-4.663542
H	-1.014152	2.875661	-5.015290
C	0.501240	5.073060	-4.816427
H	0.562160	3.633891	-3.263202
H	-0.475989	5.036305	-2.902275
O	1.003883	4.554152	-5.792483
O	0.455249	6.421118	-4.663410
H	0.902224	6.794036	-5.447049
H	-2.687284	1.214988	-4.529256
N	-3.285121	-4.063726	-0.087164
H	-3.453055	-3.275332	-0.744901
C	7.280135	1.720159	-0.460292
H	7.120314	1.506279	0.603302
H	7.854287	2.642490	-0.576042
C	5.939520	1.853676	-1.166537
O	5.599750	2.857717	-1.771367
O	5.214120	0.749304	-1.036693
C	3.194294	2.280611	-4.138383
H	3.819847	2.886220	-3.473739
H	2.587833	2.927899	-4.781221
C	2.326806	1.366109	-3.330532
N	2.793222	0.744885	-2.188605
H	4.309227	0.837742	-1.511390
C	1.795592	-0.000883	-1.738158
H	1.818210	-0.618134	-0.851018
N	0.705177	0.104450	-2.526877
H	-0.182385	-0.384295	-2.362640
C	1.024731	0.972035	-3.546780
H	0.318799	1.224615	-4.322609
H	-5.327617	-2.434872	-2.908286
H	-7.108267	0.939709	0.987759
H	-7.019696	0.603798	-1.481356
H	-1.896781	-5.314981	-4.007896
H	-3.970268	-4.283288	0.625169
H	7.837241	0.874749	-0.881839
H	3.875365	1.706665	-4.783663

Table S8. PC structure coordinates of CalB.

C	-0.423868	-3.825688	-4.913184
O	-0.552303	-4.448195	-5.955106
N	-1.075719	-4.117641	-3.740679
H	-1.099450	-3.359118	-3.063635
C	-2.140690	-5.112436	-3.725130
H	-1.803442	-5.951142	-4.340930
C	-2.461283	-5.596058	-2.311814
H	-2.866532	-4.753290	-1.720331
O	-1.338400	-6.172918	-1.665281
H	-0.585449	-5.586095	-1.848401
C	4.619310	-1.489040	-3.809811
O	4.357249	-2.597408	-4.241971
N	4.474952	-1.076973	-2.520702
H	4.708089	-0.115034	-2.315619
C	3.929847	-1.870257	-1.418955
H	4.418337	-1.499198	-0.510812
C	2.425978	-1.649107	-1.213087
H	2.150737	-2.121655	-0.255261

H	2.236487	-0.569045	-1.118447
O	1.681596	-2.197102	-2.290027
H	0.756978	-1.886804	-2.211529
C	4.414943	-3.346036	-1.517463
O	5.593516	-3.608121	-1.338972
N	3.439540	-4.285070	-1.705651
H	2.595226	-3.966327	-2.175680
C	2.248700	5.792110	5.006331
H	3.112210	5.285198	5.456098
H	1.591261	6.183385	5.790758
C	1.487822	4.833519	4.070665
O	0.243981	4.788303	4.150872
O	2.241271	4.190533	3.261020
C	-0.367959	5.288129	1.114119
H	-0.574942	5.379184	2.187246
H	-1.173688	5.729938	0.513183
C	-0.173573	3.840826	0.756874
N	0.761312	3.081482	1.415201
H	1.377495	3.462907	2.224377
C	0.704487	1.837652	0.891335
H	1.347790	1.036991	1.234879
N	-0.205879	1.722127	-0.072583
C	-0.761669	2.985318	-0.157662
H	-1.537770	3.215667	-0.876263
O	0.614900	-2.648200	4.615970
O	-3.066080	-0.784889	-1.939771
C	-0.780225	-2.504227	1.947503
C	-0.943108	-2.468719	0.422351
C	0.175737	-1.438414	2.497564
C	-1.679966	-1.203738	-0.054438
C	0.206316	-1.410092	4.028530
C	-1.864383	-1.205223	-1.538671
H	-1.770601	-2.381519	2.414288
H	-0.411775	-3.499249	2.234735
H	-1.497665	-3.361944	0.097079
H	0.038150	-2.520946	-0.063408
H	1.188681	-1.633139	2.116972
H	-0.119004	-0.442370	2.144855
H	-1.104447	-0.284050	0.155520
H	-2.653991	-1.103538	0.436297
H	0.926917	-0.663780	4.376365
H	-0.787906	-1.112645	4.403619
H	-0.056725	-3.303933	4.375873
O	-1.009800	-1.561203	-2.349391
C	-3.286790	-0.746578	-3.374933
H	-2.500643	-0.138706	-3.835416
H	-3.191030	-1.768365	-3.758642
C	-4.673465	-0.173854	-3.627343
H	-5.383221	-0.657910	-2.943231
C	-4.765862	1.352871	-3.497803
H	-5.783712	1.662479	-3.776426
C	-4.443745	1.898320	-2.103121
H	-4.089033	1.814005	-4.232400
C	-4.719534	3.409179	-2.018256
H	-3.395898	1.703836	-1.848285
H	-5.047797	1.388601	-1.343512
C	-4.406134	3.906304	-0.622998
H	-5.783391	3.594362	-2.216592
H	-4.129270	3.956566	-2.760307
O	-4.927829	3.486914	0.386479
O	-3.439431	4.853241	-0.626920
H	-3.179032	5.009913	0.302268
H	-4.963168	-0.462446	-4.646843
H	0.266518	-2.969913	-4.794970
H	-3.236324	-6.368165	-2.363053
H	-3.060872	-4.718704	-4.188290
H	5.030427	-0.676787	-4.444928
H	3.788476	-5.204375	-1.947103
H	2.642270	6.633413	4.418095
H	0.545727	5.865384	0.915513

Table S9. RC structure coordinates of AfEST.

C	66.944210	46.325720	62.705490
O	66.920792	46.828309	63.770950
N	67.958744	45.525533	62.244090
H	67.960949	45.283916	61.259016
C	69.188200	45.383459	63.022519
H	69.698799	46.343245	63.153143
H	68.930921	44.999814	64.017613
C	70.171138	44.433199	62.319759
O	71.356511	44.723902	62.193028
N	69.640087	43.256789	61.878470
H	68.637910	43.175816	61.766980
C	64.150355	43.909203	58.117803
H	63.597236	43.108862	57.603302
C	65.483376	44.097994	57.394315
H	66.116196	43.201791	57.533806
H	65.265111	44.170440	56.320120
O	66.156440	45.260857	57.840299
H	66.581914	45.668009	57.040088
C	64.145261	43.524482	59.613280
O	63.284166	43.963826	60.364183
N	65.046544	42.559406	60.045917
H	65.965324	42.551930	59.610746
C	65.494310	46.167780	49.028270
H	66.254933	46.919704	48.770280
H	64.506383	46.604646	48.843462
C	65.657045	45.794419	50.513741
O	66.558688	44.912387	50.750277
O	64.971473	46.413472	51.347747
C	67.899780	47.616418	52.018850
H	68.450515	47.036042	51.269830
H	68.451175	48.537506	52.243297
C	67.691088	46.803975	53.267883
N	67.248076	45.506336	53.186930
H	66.917237	45.091932	52.238337
C	67.084075	45.057320	54.445787
H	66.732412	44.058356	54.666726
N	67.404946	45.971121	55.361737
C	67.790233	47.074843	54.618157
H	68.103536	47.994040	55.098049
O	70.189237	42.509093	59.123989
O	68.078944	43.029594	59.473872
C	71.346927	45.209919	57.682729
C	69.821774	45.337081	57.750850
C	71.957202	44.195918	58.662224
C	69.074963	44.004937	57.509700
C	71.453821	42.766178	58.464091
C	69.049946	43.152437	58.748316
H	71.622330	44.913227	56.659442
H	71.801269	46.193371	57.858430
H	69.467021	46.026216	56.977743
H	69.512149	45.750455	58.720857
H	73.046425	44.177464	58.518662
H	71.783201	44.484687	59.708010
H	69.537673	43.470216	56.670891
H	68.044365	44.236295	57.264144
H	71.365512	42.515224	57.399718
H	72.128565	42.048009	58.936127
H	66.131820	46.419032	61.953359
H	70.169462	42.745763	61.181595
H	63.560397	44.826173	58.039892
H	65.063892	42.471397	61.055435
H	65.656946	45.300158	48.376614
H	66.923550	47.866344	51.586597

Table S10. TS_1 structure coordinates of AfEST.

C	-4.554963	1.471615	2.344716
O	-5.508538	1.976495	2.923857
N	-4.614969	0.651165	1.268633
H	-3.736628	0.370735	0.835155
C	-5.874641	0.341602	0.615822
H	-6.677857	0.540200	1.325828
H	-6.038094	1.002809	-0.250381
C	-6.039455	-1.098674	0.115857
O	-7.154833	-1.605208	0.048987
N	-4.908062	-1.741353	-0.285072
H	-4.009075	-1.276867	-0.406139
C	-0.698259	3.146883	-0.524813
H	0.300596	3.311515	-0.943335
C	-0.654798	1.944778	0.435224
H	-0.107163	2.271001	1.337987
H	-1.680069	1.708865	0.768526
O	-0.047297	0.806153	-0.108703
C	-1.671833	3.186295	-1.710604
O	-1.552072	4.056343	-2.569416
O	-0.918225	-1.056928	-1.746962
O	-2.456835	-0.281929	-0.373890
C	-1.010705	-3.703224	-0.954497
C	-1.216042	-3.140464	0.467922
C	0.292422	-3.246694	-1.635902
C	-0.753705	-1.675568	0.624872
C	0.340328	-1.723254	-1.950434
C	-1.325713	-0.801793	-0.477861
H	-1.026849	-4.799833	-0.914942
H	-1.852510	-3.406059	-1.590794
H	-0.652371	-3.745387	1.190126
H	-2.274715	-3.228363	0.742633
H	1.152885	-3.510393	-1.007372
H	0.408670	-3.810749	-2.569390
H	0.336279	-1.634113	0.621616
H	-1.090775	-1.263761	1.579043
H	1.113027	-1.209342	-1.374694
H	0.551469	-1.556680	-3.009225
N	-2.723207	2.306863	-1.713057
H	-2.628603	1.393093	-1.267922
C	8.908317	0.066274	-0.104591
H	8.925708	-0.901968	0.410854
H	9.608308	0.742835	0.391292
C	7.504478	0.622123	-0.051655
O	6.701716	-0.022420	-0.883327
O	7.176909	1.512485	0.718050
C	5.417719	-1.099133	2.079582
H	5.900223	-1.880308	1.478927
H	5.118912	-1.541484	3.036477
C	4.222443	-0.520369	1.361166
N	4.346311	0.028603	0.101683
H	5.699269	0.118127	-0.575802
C	3.136095	0.467977	-0.227552
H	2.895828	0.962851	-1.159783
N	2.216000	0.242539	0.727366
H	1.037875	0.527064	0.444025
C	2.901057	-0.392125	1.746065
H	2.407912	-0.691843	2.661240
H	-3.509045	1.636273	2.672570
H	-5.048410	-2.637227	-0.731855
H	-0.933605	4.049545	0.059090
H	-3.253526	2.321190	-2.575787
H	9.222922	-0.112799	-1.137828
H	6.163834	-0.321064	2.274323

Table S11. INT-1 structure coordinates of AfEST.

C	57.338372	35.564358	39.366536
O	57.414224	34.364468	39.613676
N	58.324365	36.359202	38.893563
H	58.127477	37.361926	38.742733
C	59.653054	35.857582	38.594351
H	60.366838	36.162237	39.377041
H	59.616438	34.766486	38.596709
C	60.276182	36.292491	37.255511
O	61.144827	35.589776	36.741702
N	59.873710	37.480567	36.737699
H	59.204409	38.119246	37.201049
C	55.425116	40.803657	39.232426
H	56.070938	41.688383	39.197221
C	56.187096	39.677826	39.974758
H	55.758083	39.547352	40.973678
H	56.091992	38.730035	39.434291
O	57.573710	39.927188	40.233057
C	54.949896	40.540761	37.780469
O	53.935064	41.103074	37.368219
O	58.381392	41.255214	38.608075
O	58.078226	39.006196	38.163257
C	61.426678	41.429744	38.816644
C	60.775972	40.745318	40.033269
C	60.476429	42.305271	37.989111
C	59.877789	39.557873	39.650920
C	59.221502	41.575042	37.509486
C	58.468140	39.881449	39.073368
H	62.264329	42.053477	39.159110
H	61.856448	40.649748	38.169120
H	60.217102	41.487251	40.612729
H	61.579176	40.368311	40.682361
H	60.150764	43.161839	38.595197
H	61.014710	42.707598	37.117200
H	59.719561	38.901100	40.514482
H	60.402008	38.962392	38.894142
H	58.643403	42.223956	36.838182
H	59.480096	40.665150	36.948318
N	55.692260	39.691746	37.016072
H	56.634682	39.398988	37.332492
C	57.865418	48.459200	44.735880
H	56.939205	48.908818	44.358705
H	58.683460	49.182025	44.685526
C	58.213546	47.224186	43.928304
O	57.203331	46.363512	43.910807
O	59.297162	47.061558	43.391156
C	59.693387	44.066729	44.653765
H	60.109689	45.015260	44.298681
H	60.503908	43.424299	45.017000
C	58.936247	43.388704	43.546092
N	57.895144	44.028988	42.902111
H	57.470742	45.496310	43.420885
C	57.452248	43.191992	41.977877
H	56.645176	43.381950	41.283851
N	58.144385	42.033967	41.990466
H	57.989111	41.244334	41.338001
C	59.096911	42.142936	42.984285
H	59.796510	41.346517	43.189399
H	56.401529	36.140508	39.517291
H	60.336732	37.766694	35.885648
H	54.515641	41.073849	39.779002
H	55.426099	39.633579	36.042644
H	57.684959	48.174214	45.779965
H	59.028404	44.294726	45.497941

Table S12. TS_2 structure coordinates of AfEST.

C	-4.676389	0.729515	2.554958
O	-5.637329	0.873909	3.298744
N	-4.698862	0.131035	1.335723
H	-3.848674	0.159224	0.775961
C	-5.924822	-0.379038	0.745277

H	-6.579710	-0.715090	1.551485
H	-6.470884	0.417886	0.217277
C	-5.796046	-1.542165	-0.251545
O	-6.802258	-2.190118	-0.525023
N	-4.591976	-1.768978	-0.840977
H	-3.730544	-1.251016	-0.665582
C	-0.977104	2.971604	-0.109247
H	-0.085980	2.484754	-0.520971
C	-1.526816	2.085313	1.019658
H	-1.309957	2.542628	1.987542
H	-2.609419	1.967657	0.935503
O	-0.907094	0.785920	1.138835
C	-1.906596	3.305167	-1.298441
O	-1.850126	4.410873	-1.828490
O	0.040506	0.064706	-1.086545
O	-2.381726	-0.106268	-0.344217
C	-0.763855	-2.829615	-1.429593
C	-0.233561	-2.632810	0.006703
C	-0.052061	-1.968071	-2.486456
C	-0.911276	-1.574989	0.900027
C	-0.293358	-0.462022	-2.351331
C	-1.316243	-0.219485	0.319514
H	-0.616736	-3.882911	-1.703613
H	-1.847176	-2.655663	-1.467743
H	0.838870	-2.420774	-0.045939
H	-0.323823	-3.582382	0.551080
H	1.026921	-2.170576	-2.434945
H	-0.378501	-2.277323	-3.490879
H	-0.273874	-1.392330	1.770224
H	-1.856372	-1.982826	1.285320
H	0.274024	0.074414	-3.129493
H	-1.355044	-0.244968	-2.530738
N	-2.759927	2.328453	-1.730206
H	-2.693799	1.376501	-1.371838
C	8.861129	1.011313	0.668716
H	9.204025	1.695365	-0.115091
H	9.708628	0.455782	1.081644
C	7.782734	0.063166	0.139669
O	6.930876	0.634549	-0.639657
O	7.762944	-1.115560	0.530616
C	5.051871	-0.904026	2.155791
H	5.962050	-1.392166	1.793617
H	4.545677	-1.546307	2.884912
C	4.136985	-0.588995	1.015949
N	4.598522	-0.182183	-0.217679
H	5.687423	0.068884	-0.479875
C	3.529994	0.047581	-0.990485
H	3.591838	0.390371	-2.013721
N	2.392723	-0.196566	-0.337391
H	1.170217	-0.073040	-0.765627
C	2.764744	-0.596323	0.928509
H	2.030970	-0.841972	1.682514
H	-3.658471	1.067694	2.829483
H	-4.574463	-2.519295	-1.517735
H	-0.668401	3.942358	0.286590
H	-3.279070	2.525212	-2.573780
H	8.428317	1.627899	1.467564
H	5.366252	0.008874	2.680427

Table S13. EAM structure coordinates of AfEST.

C	78.693724	64.836252	51.791343
O	78.870095	65.681180	50.928370
N	79.550580	64.536460	52.809366
H	79.309548	63.755638	53.408834
C	80.859196	65.159446	52.931112
H	81.651814	64.457616	52.629909
H	80.887946	65.997933	52.233225
C	81.265991	65.705862	54.309964
O	82.140237	66.561149	54.379684
N	80.670250	65.162634	55.406310
H	80.013397	64.387863	55.370185
C	75.088761	62.131979	55.023900
H	74.576141	61.482285	55.740934
C	76.449506	61.541874	54.664754
H	76.380739	60.517684	54.281222
H	76.983024	62.158825	53.938012
O	77.273328	61.410880	55.867309
C	74.994431	63.557257	55.604828
O	73.929525	63.951231	56.061018
O	81.725319	61.838871	61.377370
O	78.761536	62.942997	55.146989
C	79.379798	62.481395	59.694881
C	78.485213	62.481023	58.447075
C	79.796422	61.080293	60.159160
C	79.159600	61.801055	57.232985
C	80.517577	61.086557	61.502318
C	78.397511	62.096290	55.967636
H	80.282515	63.076006	59.507309
H	78.837049	62.980821	60.510380
H	78.231104	63.516775	58.184190
H	77.539983	61.965113	58.655577
H	78.907129	60.440880	60.255010
H	80.450439	60.611911	59.412839
H	79.203192	60.718152	57.384662
H	80.177427	62.184236	57.103778
H	79.857186	61.532841	62.266265
H	80.731844	60.049678	61.808461
H	82.158625	61.835768	62.243218
N	76.108868	64.351838	55.585127
H	76.984045	64.078389	55.155617
C	75.425352	52.157413	55.565328
H	75.540605	52.014252	54.481118
H	74.376607	51.983991	55.833488
C	75.867427	53.593274	55.934174
O	74.997942	54.439449	56.202084
O	77.136186	53.777980	55.884115
C	78.721138	54.758966	53.236375
H	78.235280	53.964705	53.814452
H	79.808610	54.663976	53.376760
C	78.204433	56.092845	53.718282
N	77.551265	56.187114	54.924229
H	77.323535	55.320289	55.509346
C	77.186986	57.478865	55.086402
H	76.628373	57.811614	55.952067
N	77.568715	58.252440	54.074237
C	78.207969	57.380121	53.211129
H	78.629673	57.725870	52.273491
H	77.776781	64.214061	51.841682
H	81.010163	65.476360	56.304832
H	74.474873	62.126151	54.113548
H	75.992224	65.307634	55.891356
H	76.068659	51.416485	56.057833
H	78.513499	54.615886	52.167597

Table S14. EAM with a **6-HCA** structure coordinates of AfEST.

C	49.669596	67.358502	48.973059
O	49.629670	67.971150	47.883804
N	49.412023	67.979768	50.121134
H	49.308841	67.392214	50.937048
C	49.141613	69.432931	50.263500
H	48.504217	69.778572	49.447332
H	48.542158	69.478725	51.173510
C	50.303326	70.345964	50.362669
O	50.135388	71.466355	50.817147
N	51.493195	69.834952	50.109757

H	51.578193	68.950793	49.627612
C	54.251128	64.753481	47.112425
H	55.053762	64.786131	46.373180
C	53.188055	65.775862	46.696256
H	52.833125	65.455293	45.715167
H	52.312782	65.749680	47.348115
O	53.537115	67.175668	46.479546
C	54.828849	64.926384	48.574675
O	55.775462	64.206978	48.922693
O	48.178748	67.464387	45.307520
O	52.466233	67.984056	48.307950
C	51.028954	68.996454	45.203824
C	51.771213	70.018977	46.125429
C	49.540477	69.502949	45.105409
C	53.184886	69.507727	46.554113
C	48.668899	68.435045	44.411354
C	53.086075	68.131846	47.256289
H	51.486876	69.052475	44.216265
H	51.046531	68.003164	45.651521
H	51.177153	70.047291	47.040777
H	51.944475	71.015727	45.717828
H	49.072329	69.717057	46.069031
H	49.410135	70.421520	44.528443
H	53.661067	70.146609	47.300471
H	53.783018	69.353301	45.657071
H	47.923035	69.125358	44.000738
H	49.198355	67.941653	43.594145
H	48.349771	67.846553	46.173469
N	54.301853	65.892540	49.388358
H	53.569968	66.523437	49.088512
C	57.176182	65.158292	37.419211
H	56.146554	65.034188	37.075717
H	57.899056	64.487072	36.952903
C	57.125808	65.062681	38.918736
O	56.031054	65.214398	39.506699
O	58.172924	64.942563	39.577129
C	54.213174	67.932654	39.367332
H	55.102069	67.447748	38.955462
H	54.247110	68.960170	38.999577
C	54.277784	67.772789	40.865534
N	54.688020	66.600892	41.449221
H	55.164791	65.893765	40.891750
C	54.499015	66.706957	42.770829
H	54.796822	65.978230	43.511614
N	53.786192	67.813412	43.037525
C	53.628001	68.481500	41.860102
H	53.151031	69.445391	41.750985
H	51.629984	73.004030	48.813988
O	52.035176	73.241442	47.964213
C	52.654901	74.478193	48.183056
H	51.974944	75.261268	48.541195
H	53.438822	74.399359	48.950555
C	53.396519	74.871077	46.895598
H	54.099258	74.066224	46.644238
C	52.526694	75.125779	45.636174
H	51.922742	74.232567	45.432057
C	51.780462	76.466911	45.738386
H	53.203919	75.104620	44.771902
C	50.849221	76.778830	44.463577
H	51.173758	76.487076	46.651284
H	52.529259	77.263617	45.820941
C	49.790428	77.884524	44.721779
H	50.291347	75.878029	44.179377
H	51.369178	77.086152	43.548103
O	50.007573	78.944184	45.291994
O	48.712489	77.786101	43.929757
H	48.052747	78.334978	44.390401
H	54.072298	75.721312	47.056103
H	49.907884	66.291959	49.005711
H	52.344190	70.470257	50.203826
H	53.852237	63.739236	47.055539
H	54.610304	65.899939	50.405720
H	57.458670	66.190192	37.193915
H	53.361354	67.401162	38.936635

Table S15. INT-2 structure coordinates of AfEST.

C	42.293242	50.904493	54.326212
O	42.362180	49.731934	54.614506
N	41.175123	51.683769	54.346620
H	41.197558	52.628518	53.945982
C	39.865053	51.135321	54.662515
H	39.270856	51.028579	53.740648
H	40.005936	50.145066	55.096392
C	39.036495	51.966044	55.657666
O	38.409266	51.424556	56.563171
N	39.013975	53.303143	55.421183
H	39.453650	53.725168	54.589295
C	43.681952	55.407232	51.622096
H	43.542652	56.219962	50.900608
C	42.702780	54.277235	51.333948
H	43.029319	53.707487	50.448955
H	42.688469	53.588461	52.189111
O	41.410730	54.815319	51.099390
C	43.625255	56.065954	53.055486
O	44.467440	56.924076	53.310771
O	43.642404	48.873316	49.399026
O	39.184497	54.853564	51.201827
C	40.482388	51.004365	49.433797
C	40.188362	52.452854	49.842957
C	41.940544	50.611218	49.688124
C	40.233596	52.673033	51.355623
C	42.276633	49.212921	49.183055
C	40.334346	54.146062	51.814748
H	39.814661	50.315027	49.973192
H	40.266730	50.880680	48.362300
H	39.209470	52.754799	49.456400
H	40.918065	53.113695	49.362864
H	42.608572	51.333059	49.199009
H	42.160259	50.652743	50.765081
H	41.093869	52.149590	51.781946
H	39.344866	52.241383	51.833140
H	41.603140	48.474201	49.652538
H	42.122568	49.154932	48.098979
H	43.796887	48.946198	50.343708
O	40.434181	54.296146	53.109783
C	38.129646	55.256446	52.057402
H	38.540134	55.702140	52.970253
H	37.585328	56.029202	51.498120
C	37.177493	54.109518	52.411218
H	36.324003	54.533904	52.962343
C	36.687329	53.331528	51.185682
H	37.552101	52.872152	50.701272
C	35.660950	52.243980	51.537357
H	36.254818	54.027990	50.450268
C	34.248652	52.815295	51.771316
H	35.985688	51.715002	52.442767
H	35.591731	51.503818	50.731678
C	33.633107	53.233643	50.452789
H	34.272495	53.661128	52.464835
H	33.598572	52.039404	52.195323
O	33.490446	52.509556	49.490766
O	33.254588	54.538677	50.434186
H	32.900242	54.701198	49.556903
H	37.685052	53.421695	53.098347
N	42.706235	55.646008	54.001045
H	41.822721	55.201723	53.691863

C	41.632291	57.571045	42.558688
H	40.566887	57.330237	42.448639
H	42.174005	57.222131	41.675764
C	42.160141	56.880106	43.801019
O	42.866147	55.888344	43.772010
O	41.704800	57.474511	44.901662
C	40.282894	54.487019	45.099394
H	39.910687	55.252745	44.403326
H	39.631471	53.609062	45.014475
C	40.303626	54.993235	46.505217
N	41.279137	55.869085	46.947856
H	41.815474	56.868599	45.715055
C	41.005973	56.102905	48.222470
H	41.585983	56.716471	48.896351
N	39.898590	55.444031	48.620512
H	39.590649	55.335093	49.598457
C	39.444322	54.722696	47.540457
H	38.583422	54.074949	47.608519
H	43.177540	51.497172	54.007949
H	38.427429	53.865701	56.021647
H	44.714626	55.053630	51.515336
H	42.687836	56.234370	54.824290
H	41.713387	58.659534	42.654461
H	41.292779	54.225347	44.769573

Table S16. PC structure coordinates of AfEST.

C	41.678230	42.261493	19.157696
O	41.847747	43.434557	19.505759
N	42.182675	41.721023	18.031837
H	41.932503	40.767534	17.811341
C	43.075256	42.445044	17.118179
H	43.850166	42.940198	17.700178
H	43.532579	41.716733	16.447982
C	42.344643	43.484639	16.247003
O	42.034826	43.258007	15.085179
N	42.109463	44.659071	16.891125
H	42.190066	44.693706	17.902784
C	41.875073	45.468296	23.032884
H	42.340103	46.183994	23.718252
C	42.950248	44.819338	22.151893
H	43.739122	44.424570	22.812242
H	42.530297	43.979140	21.591429
O	43.487808	45.734910	21.218785
H	44.183281	46.237036	21.737625
C	40.781145	46.248495	22.293641
O	40.301320	47.277457	22.753505
N	40.300137	45.685483	21.134590
H	40.875868	45.025883	20.621575
C	49.053809	49.140772	28.310492
H	49.969108	49.330925	27.731020
H	49.317460	48.539748	29.188157
C	48.040412	48.389686	27.413267
O	47.419379	49.132202	26.577778
O	47.954550	47.151792	27.540904
C	48.791022	46.848474	24.488344
H	49.289034	47.823153	24.391358
H	49.365041	46.106743	23.918859
C	47.388869	46.912923	23.982426
N	46.443903	47.702000	24.590354
H	46.686669	48.287925	25.466426
C	45.293241	47.553701	23.898130
H	44.376986	48.067681	24.157883
N	45.428442	46.713822	22.875054
C	46.746613	46.305164	22.928038
H	47.155710	45.603704	22.212783
O	45.487759	40.549838	21.610277
O	46.735273	46.264080	16.487529
C	45.425570	43.747876	19.589309
C	46.066696	45.132596	19.562048
C	45.855172	42.852698	20.752147
C	45.445072	46.024101	18.462088
C	45.018657	41.571868	20.735520
C	45.778368	45.510529	17.084361
H	45.645211	43.224705	18.650282
H	44.341207	43.895808	19.646741
H	45.877958	45.631989	20.512309
H	47.155514	45.063780	19.423213
H	46.918312	42.585678	20.674317
H	45.712997	43.383158	21.705019
H	44.358359	46.006227	18.596459
H	45.799263	47.053669	18.566834
H	43.967797	41.831230	20.951270
H	45.045925	41.129628	19.731342
H	45.541681	40.948100	22.496399
O	45.314893	44.517274	16.555481
C	47.187278	45.799798	15.202685
H	47.441020	44.735461	15.269997
H	46.373231	45.898059	14.474230
C	48.397218	46.635567	14.824102
H	49.129640	46.556800	15.637052
C	49.016359	46.174311	13.499879
H	49.290272	45.111284	13.578950
C	50.252933	46.984854	13.093766
H	48.263745	46.244254	12.702836
C	51.386834	46.868320	14.114133
H	49.987700	48.043122	12.975360
H	50.626077	46.647574	12.120673
C	52.685374	47.508793	13.644302
H	51.594788	45.808349	14.330718
H	51.101551	47.322894	15.072706
O	52.886236	47.941993	12.537843
O	53.671984	47.554766	14.584074
H	53.346612	47.183780	15.422663
H	48.108694	47.693139	14.756020
H	41.076532	41.553224	19.753231
H	41.536066	45.343956	16.417542
H	41.383487	44.697998	23.647683
H	39.702912	46.291553	20.587502
H	48.656799	50.115588	28.620619
H	48.791959	46.591908	25.554670

Supporting Information References

(1) Morris, G. M.; Huey, R.; Lindstrom, W.; Sanner, M. F.; Belew, R. K.; Goodsell, D. S.; Olson, A. J. AutoDock4 and AutoDockTools4: Automated docking with selective receptor flexibility. *J. Comput. Chem.* **2009**, 30, 2785−2791.

(2) Ryckaert, J. P.; Ciccotti, G.; Berendsen, H. J. C. Numerical integration of the cartesian equations of motion of a system with constraints: molecular dynamics of n-alkanes. *J. Comput. Phys.* **1977**, 23, 327−341.

(3) Darden, T.; York, D.; Pedersen, L. Particle mesh Ewald: An N-log(N) method for Ewald sums in large systems. *J. Chem. Phys.* **1993**, 98, 10089−10092.

(4) Carvalho, A. T. P.; Dourado, D. F. A. R.; Skvortsov, T.; de Abreu, M.; Ferguson, L. J.; Quinn, D. J.; Moody, T. S.; Huang, M. Catalytic Mechanism of Phenylacetone Monooxygenases for Non-Native Linear Substrates. *Phys. Chem. Chem. Phys.* **2017**, 19, 26851–26861.

(5) Grimme, S.; Antony, J.; Ehrlich, S.; Krieg, H. A Consistent and Accurate Ab Initio Parametrization of Density Functional Dispersion Correction (DFT-D) for the 94 Elements H-Pu. *J. Chem. Phys.* **2010**, 132, 154104.